SPG11 organoids reveal lysosomal calcium regulation of neural progenitor proliferation

Dominic Samaroo[1], Margaux Cauhape[1], Léa Bernachot[1], Alexandra Durr[1], Frédéric Darios[1].

1: Sorbonne Université, Institut du Cerveau - Paris Brain Institute - ICM, Inserm, CNRS, APHP, Hôpital de la Pitié Salpêtrière, Paris, France

Correspondance: Frédéric Darios

Paris Brain Institute - ICM

Hôpital de la Salpêtrière

47, boulevard de l'Hôpital

F-75013 France

Tel: (+33) 1 57 27 46 52

Fax: (+33) 1 57 27 46 95

E-mail: frederic.darios@icm-institute.org

Abstract

Lysosome dysfunction has been widely implicated in many models of neurodegeneration, but much less is understood of its involvement during brain development in health and disease. Hereditary spastic paraplegia caused by mutations in the *SPG11* gene is a neurodevelopmental and neurodegenerative disorder characterized by lysosome dysfunction. We identify here lysosomal accumulation of calcium in SPG11 cellular models. We show that alteration of lysosomal calcium reduced proliferation of neural progenitor cells and diminished apical tight junctions in early human cortical development, modeled using organoids derived from induced pluripotent stem cells. RNA sequencing analysis revealed that these phenotypes in SPG11 organoids are caused by hypoactivation of mTOR signaling. The latter is a consequence of lysosomal recruitment of the enzyme PI4K2A (phosphatidylinositol 4-kinase type 2 alpha) resulting in higher levels of its product PI(4)P (phosphatidylinositol-4- phosphate), a described regulator of the mTOR pathway. We observed a successful correction of all phenotypes by modulating the function of the lysosomal calcium channel TRPML1, highlighting the role of lysosomal calcium in signaling during the early phase of cortical development.

Introduction

Lysosomes are membrane-limited organelles that play a critical catabolic role, degrading the content of late endosomes and autophagosomes. However, it has emerged in the last few years that they also play important roles in signaling, acting as sensors for nutrient availability and regulating gene expression (Settembre and Perera, 2024). Besides modifying cellular homeostasis, inherited mutations affecting lysosomes have a wider impact, impairing the function of organs. This is perfectly illustrated by lysosomal storage disorders that are genetic diseases caused by deficiencies in lysosomal metabolic function and are characterized by early multisystemic alterations, which frequently include alterations of the central nervous system. These genetic disorders impact development, with symptoms beginning early in life (Allende et al., 2018; Crawley and Walkley, 2007). However, the exact physiological roles of lysosomes in organ development, notably of the brain, have still not been properly investigated (Settembre and Perera, 2024). To address this question, we used hereditary spastic paraplegia type 11 (SPG11) as a model. SPG11 is a neurodegenerative disease of genetic origin, caused by mutations in the *SPG11* gene (Stevanin et al., 2007), which is characterized by lysosomal dysfunction (Boutry et al., 2018; Chang et al., 2014; Renvoisé et al., 2014; Varga et al., 2015), and presents alterations in cortical development (Pérez-Brangulí et al., 2019; Pozner et al., 2020).

SPG11 patients present progressive spasticity of the lower limbs from the second decade of life, and is often associated with other neurological symptoms, such as ataxia, peripheral neuropathy, and cognitive impairment (Hehr et al., 2007; Stevanin et al., 2008). Neuropathological studies in autopsic brains revealed widespread neuronal death in various brain regions (Denora et al., 2016; Hayakawa et al., 2022; Krumm et al., 2024), confirming the neurodegenerative nature of the disease. However, neurodevelopmental alterations also contribute to SPG11 pathology (Pozner et al., 2020). Many SPG11 cases present low school performance predating the onset of spasticity (Faber et al., 2016). Furthermore, downregulation of *Spg11* in zebrafish demonstrates abnormal axonal branching during embryonic development, resulting in motor neuron defects (Martin et al., 2012; Southgate et al., 2010). Similarly, SPG11 patient stem cell-derived systems modeling neurodevelopment demonstrate altered proliferation of neural progenitors and premature neurogenesis, as well as disrupted signaling pathways, substantiating the role of *SPG11* during brain development (Mishra et al., 2016; Pérez-Brangulí et al., 2019; Pozner et al., 2020).

Most mutations identified in SPG11 patients are nonsense or frameshift mutations (Stevanin et al., 2008), leading to loss of function of the gene product, spatacsin. Absence of spatacsin has been largely documented to impair lysosomal function in cells and in animal models (Branchu et al., 2017; Hirst et al., 2013; Renvoisé et al., 2014; Varga et al., 2015). In particular, spatacsin is important for the regulation of autophagic lysosome reformation, a pathway crucial for lysosome membrane recycling (Chang et al., 2014; Varga et al., 2015), as well as lysosomal trafficking and motility (Pierga et al., 2023). The absence of spatacsin thus results in autolysosome accumulation, and increased intralysosomal accumulation of various lipids including cholesterol and gangliosides, which contribute to neuronal death (Boutry et al., 2019, 2018; Branchu et al., 2017; Fortier et al., 2024). Lysosomes are also known to be key players in signaling pathways, such as mTOR (Puertollano, 2014), and their dynamics have recently been shown to play a role in early cortical formation (Zou et al., 2024). However, it is not known how the loss of spatacsin impacts lysosome-dependent signaling pathways, or how the known lysosomal dysfunctions caused by the loss of spatacsin impair brain development.

Here, we used human cortical organoids to investigate the impact of spatacsin loss of function on cortical development, and the wider role of lysosomes in neurodevelopment. Our work shows that when spatacsin is absent, lysosomal calcium homeostasis is impaired with significant downstream consequences on cell signaling and neural progenitor function.

Results

Lysosomal calcium homeostasis is impaired in SPG11 neural progenitors.

We used human neural progenitor cells (NPCs) and human cortical organoids derived from induced pluripotent stem (iPS) cells as 2D and 3D models of cortical development. We first investigated the physiological functions of lysosomes that might be impaired by the loss of spatacsin. We monitored the catalytic activity of hydrolases using fluorescent reporters in NPCs derived from either the iPS cells of a healthy subject or from an isogenic iPS line in which we introduced a homozygous pathogenic nonsense mutation (c.6100C>T ; p.R2034X) into the *SPG11* gene by genome editing (Fortier et al., 2024). Control and SPG11 NPCs presented similar catabolic activity of lysosomes monitored by the DQ-BSA unquenching assay and the Magic Red Fluorescent Cathepsin B assay (Fig. 1A, Suppl. Fig. 1A). Furthermore, western blot analyses showed that the levels of the lysosomal protease Cathepsin D or the lysosome membrane protein LAMP1 were similar in control and SPG11 NPCs (Suppl. Fig. 1B-D). Together, these observations suggest that the presence of homozygous *SPG11* mutation does not change the catabolic activity of lysosomes.

Loss of spatacsin function due to *SPG11* mutations promotes accumulation of lipids, notably cholesterol in lysosomes of fibroblasts (Boutry et al., 2019). Similarly, using the cholesterol binding domain D4 of prefringolysin-O fused to GFP (GFP-D4), we observed that SPG11 NPCs presented accumulation of cholesterol in lysosomes compared to control NPCs (Fig. 1B,C). The accumulation of cholesterol in lysosomes was previously proposed to impair the function of the lysosomal calcium channel TRPML1 (Shen et al., 2012). We therefore wondered whether SPG11 NPCs may present altered calcium levels in lysosomes. To test this hypothesis, we transfected NPCs with a vector expressing the genetically encoded calcium reporter, GCaMP3, fused with the lysosomal calcium channel TRPML1 (Shen et al., 2012). To monitor the relative amount of calcium in lysosomes, lysosomal calcium store was released upon osmotic rupture of the lysosomal membrane via the peptide GPN (Morgan et al., 2015). SPG11 NPCs had higher lysosomal calcium content compared to control NPCs (Fig. 1D). To confirm this result, we incubated NPCs with the calcium probe Oregon Green Bapta coupled to 10kDa dextran and Texas Red 10kDa Dextran as a control of dye internalization. After internalization by fluid phase

endocytosis, the fluorescent probes were localized in lysosomes (Suppl. Fig. 1E). The fluorescence intensity of the calcium-sensitive Oregon Green Bapta normalized to the fluorescence intensity of Texas Red revealed a moderate but consistent increase in intralysosomal calcium in SPG11 NPCs when compared to control cells (Fig. 1F).

To show that the change in lysosomal calcium levels in SPG11 NPCs is due to cholesterol-induced changes in the activity of the TRPML1 channel (Shen et al., 2012), we triggered calcium release in GCaMP3-TRPML1 transfected NPCs by using the TRPML1 agonist ML-SA1 (X. Li et al., 2016). The response to ML-SA1 was lower in SPG11 NPCs than in control cells (Fig. 1E), suggesting that the TRPML1 channel may be less active or less functional in the absence of spatacsin, which in turn might be the cause of higher intralysosomal calcium levels in these cells. Notably, a 24 hour treatment with ML-SA1 normalized lysosomal calcium levels monitored with the Oregon Green Bapta probe in SPG11 NPCs (Fig. 1F).

Together these data show that NPCs with a homozygous *SPG11* mutation do not show alteration in catabolic activity, but present increased levels of lysosomal calcium that can be alleviated by treatment with the TRPML1 agonist ML-SA1.

Altered calcium levels contribute to lysosomal dysfunction in SPG11 cortical organoids.

To study SPG11-induced lysosomal dysfunction in neurodevelopment, we next generated human cortical organoids and performed LAMP1 immunostaining on organoids slices to label lysosomal compartments. In SPG11 cortical organoids, lysosomes accumulated at the apical (inner) surface of neural rosettes, as labelled by the tight junction protein zonula occludens-1 (ZO-1) (Fig. 2A). Quantification of the fluorescence intensity of LAMP1 along a line scan perpendicular to the apical surface of the rosettes confirmed the mislocalization of lysosomes at the apical surface of rosettes in SPG11 cortical organoids (Fig. 2B).

The accumulation of cholesterol in lysosomes and the associated impaired calcium homeostasis observed in SPG11 NPCs prompted us to investigate whether these parameters were affected in SPG11 cortical organoids. We stained organoid slices with the GFP-D4 probe that binds free cholesterol. We observed higher amounts of cholesterol in neural progenitors of SPG11 cortical organoids compared to control organoids (Fig. 2C, Suppl. Fig. 2A). In SPG11 organoids, the accumulation of cholesterol mainly occurred in lysosomes of neural progenitors (Fig. 2C,D).

To test whether these lysosomal dysfunctions were consequences of impaired lysosomal calcium levels, we evaluated the impact of chronic treatment with ML-SA1. Treatment was started after day 7 of culture and was continuous afterwards. ML-SA1 had no effect on the localization of lysosomes at the apical surface in control and SPG11 organoids (Fig. 2A,B). In contrast, in SPG11 cortical organoids, ML-SA1 treatment led to lower levels of lysosomal cholesterol (Fig. 2C,D, Suppl Fig. 2A). These data thus show that altered calcium homeostasis in SPG11 organoids contribute to accumulation of cholesterol in lysosomes.

Modulation of lysosomal calcium partially restores developmental defects in SPG11 neural progenitors in human cortical organoids

We then asked whether the previously described impaired proliferation of neural progenitor cells in cortical organoids (Pérez-Brangulí et al., 2019) might be a consequence of lysosomal dysfunctions. We stained cortical organoids differentiated for 14 days for the presence of SOX2, a marker of self-renewal. Rosettes of SPG11 cortical organoids contained noticeably fewer SOX2-positive cells than control cortical organoids (Fig. 2E-G). Treatment of SPG11 cortical organoids with ML-SA1 restored the number of SOX2-positive cells per rosette to the control condition (Fig. 2E,F). Compared to control rosettes, SPG11 rosettes showed a decrease in the proliferation of progenitors that was assessed by counting the number of SOX2-positive cells that were also positive for the proliferation marker Ki67 (Fig. 2E,G). ML-SA1 treatment restored control levels of proliferation in rosettes of SPG11 cortical organoids (Fig. 2E,G).

Proliferation of progenitor cells has been proposed to rely on proper organization of their cellular junctions (Bendriem et al., 2019; Veeraval et al., 2020). We thus monitored enrichment of tight junctions along the apical surface of rosettes using immunofluorescence of the protein ZO-1. SPG11 cortical organoids demonstrated rosettes with markedly less enriched ZO-1, with ML-SA1 treatment being able to restore levels of ZO-1 at the apical surface of rosettes in SPG11 cortical organoids (Fig. 2A, Suppl. Fig. 2B). To confirm the role of lysosomal calcium in the regulation of progenitor proliferation, we treated control and SPG11 cortical organoids with an antagonist of the TRPML1 channel, ML-SI1 (X. Li et al., 2016). ML-SI1 treatment resulted in a significant decrease in neural progenitor proliferation and ZO-1 enrichment at the apical surface of the rosette in control cortical organoids (Suppl. Fig. 2C-E).

Together, these data suggest that altered lysosomal calcium homeostasis decreases the proliferation of neural progenitor cells in cortical organoids, and that the lysosomal calcium channel agonist ML-SA1 can compensate for this dysfunction due to *SPG11* mutations.

Later stage SPG11 cortical organoids recuperate progenitor function but feature reduced neurogenesis that is improved with ML-SA1 treatment.

We then investigated the consequences of *SPG11* mutations and the impact of lysosomal calcium modulation as corticogenesis continues further, after 42 days of differentiation. At this stage, SPG11 cortical organoids presented similar levels of ZO-1 enrichment and proliferation of progenitors as control cortical organoids, even in the absence of ML-SA1 treatment (Fig. 3A-C). These observations suggest that compensatory mechanisms may occur over time in SPG11 progenitors. However, despite the normalization of progenitor proliferation in SPG11 cortical organoids, the number of SOX2-positive progenitor cells per rosette remained lower in SPG11 compared to control cortical organoids (Fig. 3D,E), which is likely a result of the lower proliferation of progenitors in the earlier phase of cortical development. Continuous treatment with ML-SA1 from day 7 in culture increased, although not significantly, the number of SOX2-positive progenitors per rosette in SPG11 cortical organoids grown for 42 days (Fig. 3D,E).

In addition to impaired proliferation, the loss of spatacsin was previously proposed to promote premature neurogenesis in cortical organoids (Pérez-Brangulí et al., 2019). 42-day-old control cortical organoids demonstrated a lamination of cortical cell types, with SOX2-positive early neural progenitors being surrounded by a layer of layer of eomesodermin (T-box brain protein 2/Tbr2) positive intermediate progenitors, and beyond that, NeuN-positive neurons. In contrast, SPG11 cortical organoids have fewer Tbr2 and NeuN-positive cells surrounding each rosette (Fig. 3D,F,G). SPG11 cortical organoids treated with ML-SA1 showed a significant increase in the number of both intermediate progenitors and neurons in laminae surrounding rosettes (Fig. 3D,F,G). Of note, ML-SA1 treated control cortical organoids had low survivability at 42 days and could not be analyzed, suggesting that chronic ML-SA1 treatment may be toxic in healthy conditions.

All together, these data suggest that, in SPG11 cortical organoids, the lower number of differentiated cells around rosettes is likely due to the observed reduction in proliferation at earlier stages, which can be compensated by treatment with ML-SA1.

mTOR signaling is dysfunctional in SPG11 neural progenitors and upregulated by ML-SA1.

We then aimed to investigate the molecular pathways linking lysosomal calcium homeostasis to proliferation of NPCs. We performed bulk RNA sequencing followed by differential analysis on 14-day-old cortical organoids, when proliferation of progenitors was impaired in SPG11 compared to control cortical organoids. We also analyzed ML-SA1 treated cortical organoids to identify genes and pathways underlying the improvements observed with treatment. Comparing SPG11 and control cortical organoids revealed 33 genes downregulated in SPG11 organoids and 57 upregulated genes (Suppl. Fig. 3A). Comparing SPG11 cortical organoids that were either untreated or treated with ML-SA1 revealed 14 genes downregulated with ML-SA1 treatment and 37 upregulated genes (Suppl. Fig. 3B).

To analyze the pathways modified either by the *SPG11* mutation or the ML-SA1 treatment, we performed a gene set enrichment analysis using gene sets from the human Molecular Signatures Database. No pathway was significantly affected at the level of gene expression between control and SPG11 organoids. In contrast, in SPG11 organoids, ML-SA1 treatment significantly modified only three hallmark genesets at the gene expression level: mTORC1 signaling, the PI3K-Akt-mTOR signaling and the p53 pathways (Suppl. Fig. 3C). Since the mTOR signaling pathway is strongly associated with lysosome function, which, according to our findings, contributes to the control of progenitor cell proliferation, we decided to focus our analysis on the impact of *SPG11* mutations and ML-SA1 on the activity of the mTOR pathway. We analyzed by immunofluorescence the phosphorylation of the ribosomal protein S6 (S6) which is a downstream effector of mTOR (Ruvinsky and Meyuhas, 2006). SPG11 cortical organoids featured significantly less phosphorylated S6 within rosettes when compared to controls, with this phosphorylation being greatly restored with ML-SA1 treatment (Fig. 4A,B).

To evaluate whether activating the mTOR signaling pathway may rescue the phenotypes observed in SPG11 organoids, we treated organoids with the mTOR agonist NV5138 (Kato et al., 2019; Sengupta et al., 2019) and we monitored by immunofluorescence the phosphorylation levels of the mTOR substrate ribosomal protein S6. NV5138 treatment significantly increased the levels of phosphorylated S6 in rosettes of 14-day-old SPG11 organoids (Fig. 4C, Suppl. Fig. 3D), suggesting that the treatment alleviated the decrease in mTOR signaling observed in SPG11 organoids. Treatment of organoids with NV5138 also significantly increased the proliferation of

neural progenitors in rosettes, as monitored by the proportion of SOX2-positive cells that were also positive for the proliferation marker Ki67 in rosettes (Fig. 4D,E). Furthermore, treatment with the mTOR agonist restored normal levels of the junction protein ZO-1 in rosettes of 14-day-old SPG11 cortical organoids (Fig. 4D,F).

Altogether, these data suggest that the downregulation of the mTOR signaling pathway observed in rosettes of SPG11 cortical organoids is responsible for the impaired proliferation and aberrant junctions in progenitors.

ML-SA1 restores mTOR signaling in SPG11 cells by modulating lysosomal levels of phosphatidylinositol-4-phosphate

To investigate the molecular mechanisms underlying the downregulation in mTOR signaling in SPG11 organoids, we used cultured NPCs as a model. Consistent with observations in organoids, SPG11 NPCs present lower levels of phosphorylated S6 as revealed by western blot, and ML-SA1 treatment led to higher levels of this phosphorylated protein in SPG11 NPCs (Fig. 5A,B). *SPG11* mutations have previously been associated with lysosomal accumulation of phosphatidylinositol 4-kinase 2α (PI4K2A) (Khundadze et al., 2021). This enzyme promotes the synthesis of the signaling lipid phosphatidylinositol-4-phosphate (PI(4)P), which contributes to repress mTORC1 signaling and inhibit its localization at the lysosomal surface (Ebner et al., 2023). We therefore hypothesized that ML-SA1 treatment modulates the mTOR pathway by modifying phosphoinositide signaling. Colocalization experiments showed that mTOR was less present on lysosomes in SPG11 compared to control NPCs, an effect that was compensated for in the presence of ML-SA1 (Fig. 5C,D). This is consistent with ML-SA1 alleviating the mTOR repression in SPG11 cells.

To evaluate whether this change in mTOR signaling was linked to lysosomal levels of PI(4)P, we expressed in NPCs the bacterial effector protein SidM (P4MSidMx2) fused to GFP as a specific optical reporter to monitor lysosomal PI(4)P (Boutry and Kim, 2021; Hammond et al., 2014). Compared to control NPCs, SPG11 NPCs presented significantly higher levels of PI(4)P signal at lysosomes labelled by Lamp1-mCherry (Fig. 5E,F). The lysosomal levels of the phosphoinositide were normalized by ML-SA1 treatment. The accumulation of PI(4)P in SPG11 NPCs was associated with higher recruitment at lysosomes of the PI(4)P synthesizing enzyme PI4K2A, an effect that was reversed by ML-SA1 treatment (Suppl. Fig. 4A,B).

Finally, to evaluate whether this pathway may contribute to the downregulation of mTOR signaling in cortical organoids, the latter were immunostained for PI4K2A. As observed in NPCs, PI4K2A was more colocalized with lysosomes in rosettes of 14-day-old SPG11 organoids compared to rosettes of control organoids, and this effect was normalized when SPG11 organoids were treated with ML-SA1 (Fig. 5G-H). Conversely, treatment of control organoids with the TRPML1 antagonist ML-SI1 significantly increased the amount of PI4K2A localized at lysosomes (Fig. 5I), suggesting that the lysosomal recruitment of this enzyme is regulated by lysosomal calcium. These data suggest that accumulation of PI4K2A on lysosomes in SPG11 NPCs contributes to altered phosphoinositide levels in this cellular compartment, regulating mTOR signaling. ML-SA1 inhibits the recruitment of PI4K2A to lysosomes, thus decreasing lysosomal levels of PI(4)P and restoring mTOR signaling.

In summary, our findings demonstrate that modulation of lysosomal calcium in cells with *SPG11* mutations prevents the accumulation of PI4K2A at lysosomes, and thus restores normal levels of PI(4)P at lysosomes, which contributes to mTOR signaling regulation. This mechanism contributes to regulation of NPC proliferation during early cortical development.

Discussion

Lysosome dysfunction has been widely implicated in many models of neurodegeneration (Darios and Stevanin, 2020; Tedesco et al., 2022; Udayar et al., 2022), but its role during brain development has not been properly investigated (Settembre and Perera, 2024). Lysosomes have emerged within recent years as a signaling hub regulating cell growth, division and differentiation (Lawrence and Zoncu, 2019), and here we have explored their role in the regulation of neural progenitor proliferation.

Our model was spatacsin loss of function associated with hereditary spastic paraplegia SPG11 causing lysosomal dysfunction (Boutry et al., 2018; Branchu et al., 2017; Chang et al., 2014; Varga et al., 2015) and neurodegeneration, as well as being linked with aberrant neurodevelopment (Martin et al., 2012; Mishra et al., 2016; Pérez-Brangulí et al., 2019; Pozner et al., 2020). Spatacsin loss of function has been associated with several lysosomal dysfunctions, such as accumulation of lipids in lysosomes (Boutry et al., 2019, 2018; Branchu et al., 2017), and impaired lysosomal trafficking (Pierga et al., 2023). Loss of spatacsin also affects autophagic

lysosome reformation, leading to the accumulation of autolysosomes (Chang et al., 2014; Varga et al., 2015), but the catalytic activity of lysosomal enzymes appears to be preserved (Chang et al., 2014). Here we identify a slight yet consistent increase in lysosomal calcium levels in cultured SPG11 NPCs, which can be compensated by a treatment with ML-SA1, an agonist of the lysosomal calcium channel TRPML1.

The normalization of cholesterol or phosphoinositide levels in lysosomes of SPG11 cortical organoids subsequent to treatment with ML-SA1 suggests that impaired lysosomal calcium homeostasis contributes to dysfunction in SPG11 cortical organoids. However, at a cellular level, the cause of this alteration to lysosomal calcium homeostasis in SPG11 is unclear. Observations in cellular models of Niemann Pick type C, which present accumulation of cholesterol, suggested a reduction in the release of lysosomal calcium mediated by the TRPML1 channel (Shen et al., 2012) could lead to higher levels of calcium in lysosomes. We also highlight in SPG11 NPCs a dysregulation in the levels of lysosomal phosphoinositides. As the lysosomal calcium channels, such as TRPML1 or TPC2, are regulated by the levels of PI(3,5)P2 (Fine et al., 2018), dysregulation of phosphoinositides may also maintain or contribute to impaired lysosomal calcium homeostasis. Alternatively, other dysregulated mechanisms could impact lysosomal calcium homeostasis (Lloyd-Evans and Waller-Evans, 2020), such as contacts between endoplasmic reticulum and lysosomes that are altered in SPG11 fibroblasts (Pierga et al., 2023) and are likely altered in SPG11 cortical organoids due to the abnormal localization of lysosomes.

In cortical organoids, a model of early cortical development (Yoon et al., 2019), we show that neural progenitor proliferation, as well as cellular junctions, are impaired in SPG11 after 14-days of differentiation. Both phenotypes can be alleviated by activating the TRPML1 channel. TRPML1-mediated calcium release is impaired in lysosomal storage disorders such as Niemann Pick type C, Niemann-Pick type A, Fabry disease, mucolipidosis type IV and Neuronal Ceroid Lipofuscinosis type 3 (Chandrachud et al., 2015; Zhong et al., 2016), which are each characterized by early onset, and possibly altered brain development (Pontillo et al., 2018; Tseng et al., 2021; Wakabayashi et al., 2011). Proliferation of neural progenitors is impaired in some models of these lysosomal storage diseases (Yang et al., 2006), but whether this dysfunction is related to impaired lysosomal calcium homeostasis still remains to be investigated. Calcium levels, and notably intracellular calcium dynamics, play a central role in the regulation of neural progenitors cell

proliferation (Díaz-Piña et al., 2024). Our work highlights the role of lysosomal calcium in the proliferation of neural progenitor cells.

Altered lysosomal calcium homeostasis has been implicated in human diseases, where it likely plays a role in signaling (Lloyd-Evans and Waller-Evans, 2020). The transcriptomic analysis, substantiated by immunohistochemistry analysis in cortical organoids suggested that the mTOR signaling pathway is inhibited in SPG11, and that the TRPML1 agonist corrects the SPG11 phenotype via the mTOR pathway activation. The latter has long been associated with impaired cortical development. Indeed, a group of neurodevelopmental disorders known as mTORopathies often presenting as cortical dysplasia associated with epilepsy have been associated with increased signaling activity of the mTOR pathway (Crino, 2015; Gerasimenko et al., 2023; Lim et al., 2015). However, hypoactivation of mTOR has also been reported as associated with abnormal cortical development (Zhang et al., 2025). Notably, pharmacological or genetic inhibition of mTOR impairs the proliferation of neural progenitors (Cloëtta et al., 2013; Romanyuk et al., 2024; Zou et al., 2024), similar to our observations in SPG11 cortical organoids. The involvement of mTOR in SPG11 is further confirmed by the corrected neural progenitor proliferation observed upon treatment of SPG11 cortical organoids with the mTOR agonist NV5138 (Kato et al., 2019; Sengupta et al., 2019; Zhang et al., 2025).

mTOR activity is regulated by a plethora of growth factors and signaling pathways. In SPG11 cortical organoids, mTOR hypoactivity is corrected by treatment with the TRPML1 agonist ML-SA1, suggesting that this decrease is due to impaired release of calcium from lysosomes. Likewise, previous studies proposed that TRPML1-mediated lysosomal calcium release is necessary for mTORC1 activity (R.-J. Li et al., 2016; Wong et al., 2012). Loss of function mutations in *SPG11* also cause lysosomal accumulation of the PI(4)P synthesizing enzyme PI4K2A (Khundadze et al., 2021). This enzyme promotes the synthesis of the signaling lipid PI(4)P, which contributes to mTORC1 signal repression (Ebner et al., 2023). Our study shows that activation of TRPML1 decreases the amount of PI4K2A localized at lysosomes in cultured neural progenitors and in cortical organoids. PI4K2A is inhibited by calcium (Baumlova et al., 2016), and thus activation of the TRPML1 channel reduces the synthesis of PI(4)P at the lysosome membranes, thereby alleviating repressed of mTOR signaling. Calcium regulation of mTOR signaling appears to be a key mechanism within mTOR regulation (Amemiya et al., 2023), and our work highlights the importance of lysosomal calcium in this process.

Limitations of the study: Our study establishes a clear link between the activity of the TRPML1 lysosomal calcium channel and impaired proliferation of progenitors at an early phase of cortical development. We identify mTOR inactivation as a pathway implicated in this pathway. However, other pathways, such as GSK3β have also been shown to be dysregulated in SPG11 (Mishra et al., 2016). GSK3β has been shown to interact with mTOR to regulate brain morphogenesis (Ka et al., 2014), and could thus also contribute to the observed phenotype. In later stage SPG11 cortical organoids, proliferation of progenitors appears to be normal, suggesting that compensatory mechanisms are likely present. Further studies are required to investigate the molecular actors involved in this innate, if imperfect, restoration of function.

Methods

Ethical Approval

The use of patient-derived material was obtained following procedures sanctioned by the ethics committee, with written and informed consent acquired from patients, as per approval of SPATAX n° DC-2008-236 - RBM029 dated 09/02/2004.

iPS cells culture

Isogenic iPS cell lines were generated by introducing a homozygous stop mutation in *SPG11* (c.6100C > T, p.R2034X) in an iPS cell line derived from an healthy subject (Fortier et al., 2024). iPS cells were cultured in mTeSR+ (STEMCELL #100-0276) medium, on Geltrex basement membrane (Gibco A1413302), at 37°C and 5% CO_2 with medium changes every 2-3 days. Cells were passaged using ReLeSR (STEMCELL #100-0483) every 4-7 days. iPS cells were stored for extended periods in liquid nitrogen using CryoStor (Sigma-Aldrich C3124) according to the manufacturer's guidelines.

Cortical Organoid Generation

Cortical organoids were generated from human iPS cells using a protocol adapted from feeder-free, xeno-free generation of cortical spheroids from human pluripotent stem cells (Yoon et al., 2019). iPS cells were detached using Gentle Cell Dissociation Reagent (STEMCELL #100-0485) for 3 minutes at 37°C, and were resuspended in 1 mL of mTeSR+ medium supplemented with 10 µM Y-27632 (+Y27) (STEMCELL #72304). The appropriate volume of cell suspension was added to the AggreWell plate to achieve a density of 3.10^6 cells per well. The plate was centrifuged at 100 x g for 1 minute, then reversed and centrifuged again at 100 x g for another 2 minutes. The plate was then incubated for 24 hours at 37°C in a 5% CO_2 incubator. On the next day, medium was removed from the AggreWell plate without disturbing the spheroids. The iPS cell-derived spheroids were harvested from the microwells by pipetting TeSR-E6 (E6) (STEMCELL #05946) medium for neural induction supplemented with SMAD inhibitors (2.5 µM Dorsomorphin [DM][STEMCELL #72102] and 10 µM SB-431542 [SB][STEMCELL #72232]) into the well. Spheroids were collected and transferred to a non-treated culture plate. The dish of cortical spheroids was then completed to a total volume of 10 mL of E6+DM+SB.

From then onwards, daily media changes were performed by removing 80-90% of the medium and replacing it with fresh medium. After 6 days, E6 medium containing DM and SB was replaced with neural medium (NM) consisting of Neurobasal-A Medium [Gibco #10888022] supplemented with B-27 minus vitamin A [1:50][Gibco #12587010], GlutaMAX [1:100][Gibco #35050038], and Antibiotic-Antimycotic [1:1000][Gibco #15240062], and further supplemented with EGF (20 ng/ml)(STEMCELL #78006) and FGF2 (20 ng/ml)(STEMCELL #78003). This medium was changed daily for the first 7 days and then every other day for the subsequent 14 days. Once organoids were 28 days old, to promote differentiation of the progenitors, FGF2 and EGF were replaced with 20 ng/mL BDNF (STEMCELL #78005) and 20 ng/mL NT-3 (STEMCELL #78074), with medium changes every other day until fixation. Treatment with ML-SA1 (TOCRIS 4746) was started at day 7 at a concentration of 20 μM and was continuous until fixation. Treatment with ML-SI1 (Sigma-Aldrich G1421) was started at day 7 at a concentration of 2 μM and was continuous until organoids were used for analysis. Treatment with NV5138 (Medchem Express HY-114384) was continuous at a concentration of 100μM from day 9 until fixation of organoids at day 14.

Generation of NPCs

NPC culture was prepared by plating a dozen 14-day-old cortical organoids into a well of a Geltrex-coated 6-well plate. The medium in the well was replenished to 2 mL using N2B27 medium (50% Neurobasal-A Medium with 50% DMEM/F-12, GlutaMAX, supplemented with 1x N-2 Supplement (Gibco 17502048), 1x B-27 supplement, w/o vitamin A, and 50 μM 2-Mercaptoethanol (Gibco 31350010)), completed with EGF2 (10 ng/ml), FGF2 (10 ng/ml), and BDNF (20 ng/ml). Daily medium changes with complete N2B27 medium were performed for 3 days until distinct neural rosettes emerged. To isolate neural rosettes, cells were rinsed with warm DMEM-F12, followed by the addition of 1 mL of STEMdiff Neural Rosette Selection Reagent (STEMCELL #05832). After a 90-minute incubation at 37°C, the selection reagent was removed and DMEM-F12 was pipetted firmly onto the neural rosettes to dislodge them. The medium containing the dislodged rosette clusters was collected in a tube, centrifuged at 200 x g for 5 minutes. The pellet was resuspended in complete N2B27 medium, ensuring minimal disruption to the rosettes, before being plated onto one well of a Geltrex-coated 6-well plate.

Daily medium changes were continued using complete N2B27 medium for 3-5 days until the rosette culture reached confluence. The passage process involved rinsing cells once with warm DMEM-F12, treating them with ACCUTASE (STEMCELL #07920) for 5 minutes, and subsequently detaching and neutralizing the detachment solution with warm N2B27 medium. After centrifugation at 180 x g for 4 minutes, the cells were resuspended in N2B27 complete medium and seeded onto Geltrex-coated cultureware at a density of 150,000 cells/cm^2. NPC identity was confirmed via immunofluorescence of markers PAX6, SOX-2, and Nestin. NPCs were used until they reached passage 10.

Immunostaining

At specified time points, organoids were fixed in 4% paraformaldehyde (PFA) diluted in PBS for 24 hours, then cryoconserved by submerging 24 hours in 30% sucrose (Sigma-Aldrich S0389), and embedded in Neg-50 Frozen Section Medium (Epredia 6502) before being stored at -80°C. Organoid slices (12 µm) were cut on a cryostat (LEICA_CM3050S) and mounted on Superfrost slides (Epredia J1800AMNZ) before being stored at -80°C. To perform immunostaining, slides were thawed for 30 minutes, and rehydrated in 1x PBS (EUROMEDEX ET330A) for 5 minutes. Blocking was performed with 1x PBS, Triton X-100 0.1% (Sigma-Aldrich T9284), and 3% BSA (EUROMEDEX ET330A 04-100-812) for 1 hour. Primary antibody solution was prepared in the same solution as during blocking and applied to slides overnight at 4°C. After three washes with PBS 1x, secondary antibodies, also in blocking solution, were applied for 1 hour. Slides were washed three times with PBS, and mounted on glass slides with Fluoromount (Sigma-Aldrich F4680).

To perform immunostaining on NPCs, cells were fixed with PFA 4% diluted in PBS for 30 minutes. Immunostaining of NPCs was performed as with organoids, except initial blocking was 30 minutes, and primary antibody incubation was 1 hour.

Transcriptomic analysis of organoids

RNA was purified from fresh d14 hCOs using Maxwell RSC simplyRNA Cells Kit (Promega AS1390) for the Maxwell RSC Instrument. mRNA library preparation was realized following manufacturer's recommendations (ILLUMINA mRNA prep). Final samples pooled library preparations were sequenced on Nextseq 2000 ILLUMINA with P2-200cycles cartridge

(2x400Millions of 100 bases reads), corresponding to 2 x 25 million reads per sample after demultiplexing. Raw data was processed with Dragen Illumina DRAGEN bio-IT Platform (v3.10.11), using default parameters, for adapter trimming, alignment to the hg38 reference genome with the gencode v37 gtf file and expression quantification. Library orientation, library composition and coverage along transcripts were checked with Picard tools.

Downstream analyses were conducted with R (v4.1.1) via an interface provided by the Data Analysis Core of the Paris Brain Institute. Cpm-normalization was performed with edgeR (v3.28.0) for initial filtering (cpm > 1 in at least 1 sample). Differential analysis was performed with EdgeR, with thresholds on log2 fold change > 1 and FDR < 0.05. Experiments launched separately were added as a covariate to account for experimental variation. P-values were adjusted with the Benjamini-Hochberg procedure to control for multiple hypotheses testing. Enrichment analysis was conducted with clusterProfiler R package (v4.2.2) (Yu et al., 2012) with Gene Set Enrichment Analysis, on *a priori* identified pathways from the HALLMARK database.

Antibodies and Fluorescent Molecules

Antibodies used include: anti-SOX2 (Invitrogen 14-9811-82), anti-ZO-1 (Cell Signaling Technology #13663), mouse anti-LAMP-1 (Santa Cruz sc-18821), rabbit anti-LAMP1 (Cell Signaling Technology #9091), anti-Ki-67 (BD 550609), anti-NeuN (Sigma-Aldrich MAB377), anti-Tbr2 (Sigma-Aldrich AB2283), anti-Phospho-S6 Ribosomal Protein (Ser240/244) (Cell Signaling Technology #5364), anti-S6 Ribosomal Protein (Cell Signaling Technology #2317), anti-PI4K2A (Santa Cruz Biotechnology sc-390026), anti-mTOR (Cell Signaling Technology #2983), anti-Cathepsin D (Abcam #ab75852), anti-β-tubulin (Abcam #ab6046) and anti-GAPDH (Sigma-Aldrich #G9545). To stain nuclei we used DAPI dilactate (Sigma-Aldrich D9564).

Plasmids

The vector expressing the calcium probe GCaMP3 fused to TRPML1 (GCaMP3-TRPML1) (Shen et al., 2012) was obtained from Haoxing Xu (University of Michigan, USA). GFP-P4M-SidMx2 (#51472), Lamp1-mCherry (#45147) were obtained from Addgene. Plasmid allowing production of the GFP-D4 probe (Abe and Kobayashi, 2017) was a gift from T. Kobayashi (CNRS, Illkrich, France).

Western Blot

Cells were detached with ACCUTASE, washed once with PBS, and suspended in lysis buffer (100mM NaCl, 10 mM TRIS pH 7.4, 2 mM $MgCl_2$, 1% SDS, 0.1% Benzonase). The suspension was then centrifuged at 17,000g for 15 minutes at room temperature, and the supernatant was collected. 20 µg of protein were loaded and separated on NuPAGE 4%-12% gels (Invitrogen NP0321) in NuPAGE MOPS (Invitrogen NP0001) buffer. Protein was transferred to Immobilon-PVDF (Millipore IPVH00010) membranes. Membranes were saturated with 5% semi-skimmed milk diluted in PBS-0.5% Tween20 for 30 minutes, followed by incubation with primary antibodies in the same solution overnight at 4°C. The following day, the membrane was washed and incubated with secondary antibodies coupled to HRP (The Jackson Laboratory) in milk for 1 hour before being imaged using SuperSignal West Femto (Thermofisher 34075/34094) with a ChemiDoc Touch system (Bio-Rad).

Lysosomal Calcium Assay

To monitor lysosomal calcium, NPCs were grown in Nunc Lab-TekII chambers (Thermo Scientific 171080) and were transfected with a vector expressing the calcium probe GCaMP3 fused to TRPML1 that preferentially detects juxta-lysosomal Ca^{2+} increases (Shen et al., 2012). 10^6 cells were transfected with 5 µg of plasmid using the Neon electroporation system (Invitrogen NEON) with 3 pulses of 10 ms at 1300V according to manufacturer's instructions, and were analyzed 24 hours later. To induce the release of calcium from lysosomes, we performed live imaging in a thermostated chamber with a Leica DMi8 inverted microscope equipped with 63× objective N.A. 1.40, a Yokogawa Confocal Spinning Disk module and a Hamamatsu Orca flash 4.0 camera. We measured changes in the fluorescence of the GCaMP3-TRPML1 probe upon addition of 200 µM GPN (Abcam, ab145914) which induces the release of lysosomal calcium upon osmotic shock causing lysosome membrane permeability, or upon addition of 20 µM ML-SA1 which induces the release of calcium through the TRPML1 channel.

As an alternative method to monitor lysosomal calcium, NPCs grown on 8-chamber Ibidi coverglass at a density of 50,000 cells/cm2 were incubated with 0.1 mg/mL of 10 kDa dextran coupled to calcium-sensitive Oregon Green 488 BAPTA-1 (Invitrogen O6798) and 0.1 mg/mL 10 kDa Dextran coupled to Texas Red (Invitrogen D1830) overnight to allow the dyes to reach late endosomes and lysosomes upon endocytosis. The following day, the medium was changed 6 hours

before analysis to clear out the excess dye. Thirty minutes before analysis, the medium was replaced with DMEM without phenol red (Gibco A1443001) supplemented either with 50 nM CellTracker Blue (Invitrogen C2110) for 30 minutes to stain the cytoplasm, or with 50nM Lysotracker blue DND-22 (Invitrogen L7525) for 30 minutes to stain lysosomes. After a wash with DMEM without phenol red, we performed live imaging at 37°C and 5% CO_2 with a Leica DMi8 inverted microscope equipped with 63× objective N.A. 1.40, a Yokogawa Confocal Spinning Disk module and a Hamamatsu Orca flash 4.0 camera. Lysosomal calcium was assessed by normalizing the fluorescence value of calcium-sensitive BAPTA-1 Oregon Green to the fluorescence value of Texas Red in randomly selected cells.

Lysosomal catalytic activity assays

Lysosomal catalytic activity was assessed in control and SPG11 NPCs using two independent assays, the magic red fluorescent cathepsin B and the DQ-BSA assay. NPCs were incubated with CellTracker™ Blue at 37°C for 30 minutes. Next, cells were incubated in medium containing Magic Red Fluorescent Cathepsin B (ImmunoChemistry Technologies 937) for 60 minutes. Finally, cells were rinsed with PBS once, fixed with 4% PFA, and then imaged with an automated ArrayScan XTI (ThermoScientific) using the General Intensity Measurement protocol, analyzing > 500 cells per well and per set of conditions.

For the second assay, cells were incubated with 5µg/ml DQ Green BSA (Thermofisher) for 1 hour at 37°C. Cells were then fixed and imaged using a with a Leica DMi8 inverted microscope equipped with 63× objective N.A. 1.40, a Yokogawa Confocal Spinning Disk module and a Hamamatsu Orca flash 4.0 camera. Signal intensity was monitored using FiJi.

Cholesterol staining

Cholesterol was stained using a preparation of domain D4 of prefringolysin O fused to GFP (GFP-D4) that was produced and purified as previously described (Abe and Kobayashi, 2017). Cells or organoid slices were first processed for immunostaining with LAMP1 antibody. Labeling of cholesterol was performed by incubating samples with 20 µg/ml recombinant GFP-D4 for 20 min at 22 °C.

Image Analysis

Image analysis was performed using FiJi. Proliferation of progenitors was quantified by counting the number of Ki-67 positive and Sox2 positive nuclei within the first layer of cells around the rosette apical surface (as indicated by ZO-1), and dividing by the total number of SOX2 positive nuclei in the same layer of cells around the rosette apical surface. Neurogenesis was assessed by counting the number of Tbr2 and NeuN positive nuclei within the vicinity of each rosette.

To monitor enrichment of tight junction marker and lysosomes at the apical surface of organoid rosettes, we measured the fluorescence intensity of the immunostaining of ZO-1 and LAMP1, respectively, across a 3 μm-wide line perpendicular to the apical surface using the Plot profile tool in FiJi. Values were normalized to the average minimum and maximum values in control organoids of each experiment.

Fluorescence intensity of cells stained with DQ-BSA, Oregon Green 488 BAPTA-1-dextran, Texas Red-dextran and GFP-D4 (cholesterol levels), or transfected with the GCaMP3-TRPML1 probe were quantified as the mean gray value using FiJi. Colocalization of cholesterol staining (GFP-D4) with lysosomes was quantified using FiJi on images of randomly selected cells or rosettes as previously described (Boutry et al., 2019). First, we created a mask corresponding to LAMP1 staining in each rosette using the IJ_IsoData threshold in FiJi. The mask was copied to the corresponding fluorescence image of cholesterol. We quantified the total intensity of cholesterol fluorescence in the lysosome mask and expressed it as the percentage of total cholesterol fluorescence in every cell or rosette. The same method was applied to mTOR and PI4K2A immunostainings.

Intensity of bands in western blot was quantified using the Gel tool in FiJi.

Statistics

With the exception of the previously described transcriptomic analyses, all statistics were performed using GraphPad Prism version 10.2.0 (https://www.graphpad.com/). Tests performed are described in each figure description.

Acknowledgments

This work benefited from equipment and services from the iGenSeq (genotyping and sequencing), ICV-iPS (cell culture), HISTOMICS (histology), ICM.Quant (microscopy; RRID: SCR_026393) and Data Analysis Core (DAC) facilities at the Paris Brain Institute (ICM). We gratefully acknowledge Marie Coutelier and Simang Champramary for their assistance with RNAseq data analysis. This work was supported by the "Investissements d'avenir" program grants (ANR-10-IAIHU-06) and (ANR-11-INBS-0011). The project was also supported by a FRM Equipe funding (EQU202203014671 to A.D.). D.S. was supported by a grant from the ED3C doctoral School (Sorbonne Université).

References

Abe, M., Kobayashi, T., 2017. Dynamics of sphingomyelin- and cholesterol-enriched lipid domains during cytokinesis. Methods Cell Biol 137, 15–24. https://doi.org/10.1016/bs.mcb.2016.03.030

Allende, M.L., Cook, E.K., Larman, B.C., Nugent, A., Brady, J.M., Golebiowski, D., Sena-Esteves, M., Tifft, C.J., Proia, R.L., 2018. Cerebral organoids derived from Sandhoff disease-induced pluripotent stem cells exhibit impaired neurodifferentiation. J Lipid Res 59, 550–563. https://doi.org/10.1194/jlr.M081323

Amemiya, Y., Maki, M., Shibata, H., Takahara, T., 2023. New Insights into the Regulation of mTOR Signaling via Ca2+-Binding Proteins. Int J Mol Sci 24, 3923. https://doi.org/10.3390/ijms24043923

Baumlova, A., Gregor, J., Boura, E., 2016. The structural basis for calcium inhibition of lipid kinase PI4K IIalpha and comparison with the apo state. Physiol Res 65, 987–993. https://doi.org/10.33549/physiolres.933344

Bendriem, R.M., Singh, S., Aleem, A.A., Antonetti, D.A., Ross, M.E., 2019. Tight junction protein occludin regulates progenitor Self-Renewal and survival in developing cortex. Elife 8, e49376. https://doi.org/10.7554/eLife.49376

Boutry, M., Branchu, J., Lustremant, C., Pujol, C., Pernelle, J., Matusiak, R., Seyer, A., Poirel, M., Chu-Van, E., Pierga, A., Dobrenis, K., Puech, J.-P., Caillaud, C., Durr, A., Brice, A., Colsch, B., Mochel, F., El Hachimi, K.H., Stevanin, G., Darios, F., 2018. Inhibition of Lysosome Membrane Recycling Causes Accumulation of Gangliosides that Contribute to Neurodegeneration. Cell Reports 23, 3813–3826. https://doi.org/10.1016/j.celrep.2018.05.098

Boutry, M., Kim, P.K., 2021. ORP1L mediated PI(4)P signaling at ER-lysosome-mitochondrion three-way contact contributes to mitochondrial division. Nat Commun 12, 5354. https://doi.org/10.1038/s41467-021-25621-4

Boutry, M., Pierga, A., Matusiak, R., Branchu, J., Houllegatte, M., Ibrahim, Y., Balse, E., El Hachimi, K.-H., Brice, A., Stevanin, G., Darios, F., 2019. Loss of spatacsin impairs cholesterol trafficking and calcium homeostasis. Commun Biol 2, 380. https://doi.org/10.1038/s42003-019-0615-z

Branchu, J., Boutry, M., Sourd, L., Depp, M., Leone, C., Corriger, A., Vallucci, M., Esteves, T., Matusiak, R., Dumont, M., Muriel, M.-P., Santorelli, F.M., Brice, A., El Hachimi, K.H.,

Stevanin, G., Darios, F., 2017. Loss of spatacsin function alters lysosomal lipid clearance leading to upper and lower motor neuron degeneration. Neurobiology of Disease 102, 21–37. https://doi.org/10.1016/j.nbd.2017.02.007

Chandrachud, U., Walker, M.W., Simas, A.M., Heetveld, S., Petcherski, A., Klein, M., Oh, H., Wolf, P., Zhao, W.-N., Norton, S., Haggarty, S.J., Lloyd-Evans, E., Cotman, S.L., 2015. Unbiased Cell-based Screening in a Neuronal Cell Model of Batten Disease Highlights an Interaction between Ca2+ Homeostasis, Autophagy, and CLN3 Protein Function. J Biol Chem 290, 14361–14380. https://doi.org/10.1074/jbc.M114.621706

Chang, J., Lee, S., Blackstone, C., 2014. Spastic paraplegia proteins spastizin and spatacsin mediate autophagic lysosome reformation. J. Clin. Invest. 124, 5249–5262. https://doi.org/10.1172/JCI77598

Cloëtta, D., Thomanetz, V., Baranek, C., Lustenberger, R.M., Lin, S., Oliveri, F., Atanasoski, S., Rüegg, M.A., 2013. Inactivation of mTORC1 in the developing brain causes microcephaly and affects gliogenesis. J Neurosci 33, 7799–7810. https://doi.org/10.1523/JNEUROSCI.3294-12.2013

Crawley, A.C., Walkley, S.U., 2007. Developmental analysis of CNS pathology in the lysosomal storage disease alpha-mannosidosis. J Neuropathol Exp Neurol 66, 687–697. https://doi.org/10.1097/nen.0b013e31812503b6

Crino, P.B., 2015. mTOR signaling in epilepsy: insights from malformations of cortical development. Cold Spring Harb Perspect Med 5, a022442. https://doi.org/10.1101/cshperspect.a022442

Darios, F., Stevanin, G., 2020. Impairment of Lysosome Function and Autophagy in Rare Neurodegenerative Diseases. J Mol Biol 432, 2714–2734. https://doi.org/10.1016/j.jmb.2020.02.033

Denora, P.S., Smets, K., Zolfanelli, F., Ceuterick-de Groote, C., Casali, C., Deconinck, T., Sieben, A., Gonzales, M., Zuchner, S., Darios, F., Peeters, D., Brice, A., Malandrini, A., De Jonghe, P., Santorelli, F.M., Stevanin, G., Martin, J.-J., El Hachimi, K.H., 2016. Motor neuron degeneration in spastic paraplegia 11 mimics amyotrophic lateral sclerosis lesions. Brain aww061. https://doi.org/10.1093/brain/aww061

Díaz-Piña, D.A., Rivera-Ramírez, N., García-López, G., Díaz, N.F., Molina-Hernández, A., 2024. Calcium and Neural Stem Cell Proliferation. Int J Mol Sci 25, 4073. https://doi.org/10.3390/ijms25074073

Ebner, M., Puchkov, D., López-Ortega, O., Muthukottiappan, P., Su, Y., Schmied, C., Zillmann, S., Nikonenko, I., Koddebusch, J., Dornan, G.L., Lucht, M.T., Koka, V., Jang, W., Koch, P.A., Wallroth, A., Lehmann, M., Brügger, B., Pende, M., Winter, D., Haucke, V., 2023. Nutrient-regulated control of lysosome function by signaling lipid conversion. Cell 186, 5328-5346.e26. https://doi.org/10.1016/j.cell.2023.09.027

Faber, I., Branco, L.M.T., França Júnior, M.C., 2016. Cognitive dysfunction in hereditary spastic paraplegias and other motor neuron disorders. Dement Neuropsychol 10, 276–279. https://doi.org/10.1590/s1980-5764-2016dn1004004

Fine, M., Schmiege, P., Li, X., 2018. Structural basis for PtdInsP2-mediated human TRPML1 regulation. Nat Commun 9, 4192. https://doi.org/10.1038/s41467-018-06493-7

Fortier, M., Cauhapé, M., Buono, S., Becker, J., Menuet, A., Branchu, J., Ricca, I., Mero, S., Dorgham, K., El Hachimi, K.-H., Dobrenis, K., Colsch, B., Samaroo, D., Devaux, M., Durr, A., Stevanin, G., Santorelli, F.M., Colombo, S., Cowling, B., Darios, F., 2024.

Decreasing ganglioside synthesis delays motor and cognitive symptom onset in Spg11 knockout mice. Neurobiol Dis 199, 106564. https://doi.org/10.1016/j.nbd.2024.106564
Gerasimenko, A., Baldassari, S., Baulac, S., 2023. mTOR pathway: Insights into an established pathway for brain mosaicism in epilepsy. Neurobiol Dis 182, 106144. https://doi.org/10.1016/j.nbd.2023.106144
Hammond, G.R.V., Machner, M.P., Balla, T., 2014. A novel probe for phosphatidylinositol 4-phosphate reveals multiple pools beyond the Golgi. J Cell Biol 205, 113–126. https://doi.org/10.1083/jcb.201312072
Hayakawa, M., Matsubara, T., Mochizuki, Y., Takeuchi, C., Minamitani, M., Imai, M., Kosaki, K., Arai, T., Murayama, S., 2022. An autopsied case report of spastic paraplegia with thin corpus callosum carrying a novel mutation in the SPG11 gene: widespread degeneration with eosinophilic inclusions. BMC Neurol 22, 2. https://doi.org/10.1186/s12883-021-02514-z
Hehr, U., Bauer, P., Winner, B., Schule, R., Olmez, A., Koehler, W., Uyanik, G., Engel, A., Lenz, D., Seibel, A., Hehr, A., Ploetz, S., Gamez, J., Rolfs, A., Weis, J., Ringer, T.M., Bonin, M., Schuierer, G., Marienhagen, J., Bogdahn, U., Weber, B.H.F., Topaloglu, H., Schols, L., Riess, O., Winkler, J., 2007. Long-term course and mutational spectrum of spatacsin-linked spastic paraplegia. Ann. Neurol. 62, 656–665. https://doi.org/10.1002/ana.21310
Hirst, J., Borner, G.H.H., Edgar, J., Hein, M.Y., Mann, M., Buchholz, F., Antrobus, R., Robinson, M.S., 2013. Interaction between AP-5 and the hereditary spastic paraplegia proteins SPG11 and SPG15. Mol Biol Cell 24, 2558–2569. https://doi.org/10.1091/mbc.E13-03-0170
Ka, M., Condorelli, G., Woodgett, J.R., Kim, W.-Y., 2014. mTOR regulates brain morphogenesis by mediating GSK3 signaling. Development 141, 4076–4086. https://doi.org/10.1242/dev.108282
Kato, T., Pothula, S., Liu, R.-J., Duman, C.H., Terwilliger, R., Vlasuk, G.P., Saiah, E., Hahm, S., Duman, R.S., 2019. Sestrin modulator NV-5138 produces rapid antidepressant effects via direct mTORC1 activation. J Clin Invest 129, 2542–2554. https://doi.org/10.1172/JCI126859
Khundadze, M., Ribaudo, F., Hussain, A., Stahlberg, H., Brocke-Ahmadinejad, N., Franzka, P., Varga, R.-E., Zarkovic, M., Pungsrinont, T., Kokal, M., Ganley, I.G., Beetz, C., Sylvester, M., Hübner, C.A., 2021. Mouse models for hereditary spastic paraplegia uncover a role of PI4K2A in autophagic lysosome reformation. Autophagy 17, 3690–3706. https://doi.org/10.1080/15548627.2021.1891848
Krumm, L., Pozner, T., Zagha, N., Coras, R., Arnold, P., Tsaktanis, T., Scherpelz, K., Davis, M.Y., Kaindl, J., Stolzer, I., Süß, P., Khundadze, M., Hübner, C.A., Riemenschneider, M.J., Baets, J., Günther, C., Jayadev, S., Rothhammer, V., Krach, F., Winkler, J., Winner, B., Regensburger, M., 2024. Neuroinflammatory disease signatures in SPG11-related hereditary spastic paraplegia patients. Acta Neuropathol 147, 28. https://doi.org/10.1007/s00401-023-02675-w
Lawrence, R.E., Zoncu, R., 2019. The lysosome as a cellular centre for signalling, metabolism and quality control. Nat Cell Biol 21, 133–142. https://doi.org/10.1038/s41556-018-0244-7

Li, R.-J., Xu, J., Fu, C., Zhang, J., Zheng, Y.G., Jia, H., Liu, J.O., 2016. Regulation of mTORC1 by lysosomal calcium and calmodulin. eLife 5, e19360. https://doi.org/10.7554/eLife.19360

Li, X., Rydzewski, N., Hider, A., Zhang, X., Yang, J., Wang, W., Gao, Q., Cheng, X., Xu, H., 2016. A molecular mechanism to regulate lysosome motility for lysosome positioning and tubulation. Nat Cell Biol 18, 404–417. https://doi.org/10.1038/ncb3324

Lim, J.S., Kim, W., Kang, H.-C., Kim, S.H., Park, A.H., Park, E.K., Cho, Y.-W., Kim, S., Kim, H.M., Kim, J.A., Kim, J., Rhee, H., Kang, S.-G., Kim, H.D., Kim, D., Kim, D.-S., Lee, J.H., 2015. Brain somatic mutations in MTOR cause focal cortical dysplasia type II leading to intractable epilepsy. Nat Med 21, 395–400. https://doi.org/10.1038/nm.3824

Lloyd-Evans, E., Waller-Evans, H., 2020. Lysosomal Ca2+ Homeostasis and Signaling in Health and Disease. Cold Spring Harb Perspect Biol 12, a035311. https://doi.org/10.1101/cshperspect.a035311

Martin, E., Yanicostas, C., Rastetter, A., Alavi Naini, S.M., Maouedj, A., Kabashi, E., Rivaud-Péchoux, S., Brice, A., Stevanin, G., Soussi-Yanicostas, N., 2012. Spatacsin and spastizin act in the same pathway required for proper spinal motor neuron axon outgrowth in zebrafish. Neurobiol Dis 48, 299–308. https://doi.org/10.1016/j.nbd.2012.07.003

Mishra, H.K., Prots, I., Havlicek, S., Kohl, Z., Perez-Branguli, F., Boerstler, T., Anneser, L., Minakaki, G., Wend, H., Hampl, M., Leone, M., Brückner, M., Klucken, J., Reis, A., Boyer, L., Schuierer, G., Behrens, J., Lampert, A., Engel, F.B., Gage, F.H., Winkler, J., Winner, B., 2016. GSK3ß-dependent dysregulation of neurodevelopment in SPG11-patient induced pluripotent stem cell model: Neurodevelopmental defects in motor neuron disease. Ann Neurol. 79, 826–840. https://doi.org/10.1002/ana.24633

Morgan, A.J., Davis, L.C., Galione, A., 2015. Imaging approaches to measuring lysosomal calcium. Methods Cell Biol 126, 159–195. https://doi.org/10.1016/bs.mcb.2014.10.031

Pérez-Brangulí, F., Buchsbaum, I.Y., Pozner, T., Regensburger, M., Fan, W., Schray, A., Börstler, T., Mishra, H., Gräf, D., Kohl, Z., Winkler, J., Berninger, B., Cappello, S., Winner, B., 2019. Human SPG11 cerebral organoids reveal cortical neurogenesis impairment. Human Molecular Genetics 28, 961–971. https://doi.org/10.1093/hmg/ddy397

Pierga, A., Matusiak, R., Cauhapé, M., Branchu, J., Danglot, L., Boutry, M., Darios, F., 2023. Spatacsin regulates directionality of lysosome trafficking by promoting the degradation of its partner AP5Z1. PLoS Biol 21, e3002337. https://doi.org/10.1371/journal.pbio.3002337

Pontillo, G., Cocozza, S., Brunetti, A., Brescia Morra, V., Riccio, E., Russo, C., Saccà, F., Tedeschi, E., Pisani, A., Quarantelli, M., 2018. Reduced Intracranial Volume in Fabry Disease: Evidence of Abnormal Neurodevelopment? Front Neurol 9, 672. https://doi.org/10.3389/fneur.2018.00672

Pozner, T., Regensburger, M., Engelhorn, T., Winkler, J., Winner, B., 2020. Janus-faced spatacsin (SPG11): involvement in neurodevelopment and multisystem neurodegeneration. Brain 143, 2369–2379. https://doi.org/10.1093/brain/awaa099

Puertollano, R., 2014. mTOR and lysosome regulation. F1000Prime Rep 6. https://doi.org/10.12703/P6-52

Renvoisé, B., Chang, J., Singh, R., Yonekawa, S., FitzGibbon, E.J., Mankodi, A., Vanderver, A., Schindler, A.B., Toro, C., Gahl, W.A., Mahuran, D.J., Blackstone, C., Pierson, T.M.,

2014. Lysosomal abnormalities in hereditary spastic paraplegia types SPG15 and SPG11. Ann Clin Transl Neurol 1, 379–389. https://doi.org/10.1002/acn3.64

Romanyuk, N., Sintakova, K., Arzhanov, I., Horak, M., Gandhi, C., Jhanwar-Uniyal, M., Jendelova, P., 2024. mTOR pathway inhibition alters proliferation as well as differentiation of neural stem cells. Front Cell Neurosci 18, 1298182. https://doi.org/10.3389/fncel.2024.1298182

Ruvinsky, I., Meyuhas, O., 2006. Ribosomal protein S6 phosphorylation: from protein synthesis to cell size. Trends Biochem Sci 31, 342–348. https://doi.org/10.1016/j.tibs.2006.04.003

Sengupta, S., Giaime, E., Narayan, S., Hahm, S., Howell, J., O'Neill, D., Vlasuk, G.P., Saiah, E., 2019. Discovery of NV-5138, the first selective Brain mTORC1 activator. Sci Rep 9, 4107. https://doi.org/10.1038/s41598-019-40693-5

Settembre, C., Perera, R.M., 2024. Lysosomes as coordinators of cellular catabolism, metabolic signalling and organ physiology. Nat Rev Mol Cell Biol 25, 223–245. https://doi.org/10.1038/s41580-023-00676-x

Shen, D., Wang, X., Li, X., Zhang, X., Yao, Z., Dibble, S., Dong, X., Yu, T., Lieberman, A.P., Showalter, H.D., Xu, H., 2012. Lipid storage disorders block lysosomal trafficking by inhibiting a TRP channel and lysosomal calcium release. Nat Commun 3, 731. https://doi.org/10.1038/ncomms1735

Southgate, L., Dafou, D., Hoyle, J., Li, N., Kinning, E., Critchley, P., Németh, A.H., Talbot, K., Bindu, P.S., Sinha, S., Taly, A.B., Raghavendra, S., Müller, F., Maher, E.R., Trembath, R.C., 2010. Novel SPG11 mutations in Asian kindreds and disruption of spatacsin function in the zebrafish. Neurogenetics 11, 379–389. https://doi.org/10.1007/s10048-010-0243-8

Stevanin, G., Azzedine, H., Denora, P., Boukhris, A., Tazir, M., Lossos, A., Rosa, A.L., Lerer, I., Hamri, A., Alegria, P., Loureiro, J., Tada, M., Hannequin, D., Anheim, M., Goizet, C., Gonzalez-Martinez, V., Le Ber, I., Forlani, S., Iwabuchi, K., Meiner, V., Uyanik, G., Erichsen, A.K., Feki, I., Pasquier, F., Belarbi, S., Cruz, V.T., Depienne, C., Truchetto, J., Garrigues, G., Tallaksen, C., Tranchant, C., Nishizawa, M., Vale, J., Coutinho, P., Santorelli, F.M., Mhiri, C., Brice, A., Durr, A., 2008. Mutations in SPG11 are frequent in autosomal recessive spastic paraplegia with thin corpus callosum, cognitive decline and lower motor neuron degeneration. Brain 131, 772–784. https://doi.org/10.1093/brain/awm293

Stevanin, G., Santorelli, F.M., Azzedine, H., Coutinho, P., Chomilier, J., Denora, P.S., Martin, E., Ouvrard-Hernandez, A.-M., Tessa, A., Bouslam, N., Lossos, A., Charles, P., Loureiro, J.L., Elleuch, N., Confavreux, C., Cruz, V.T., Ruberg, M., Leguern, E., Grid, D., Tazir, M., Fontaine, B., Filla, A., Bertini, E., Durr, A., Brice, A., 2007. Mutations in SPG11, encoding spatacsin, are a major cause of spastic paraplegia with thin corpus callosum. Nat Genet 39, 366–372. https://doi.org/10.1038/ng1980

Tedesco, B., Ferrari, V., Cozzi, M., Chierichetti, M., Casarotto, E., Pramaggiore, P., Mina, F., Piccolella, M., Cristofani, R., Crippa, V., Rusmini, P., Galbiati, M., Poletti, A., 2022. The role of autophagy-lysosomal pathway in motor neuron diseases. Biochem Soc Trans 50, 1489–1503. https://doi.org/10.1042/BST20220778

Tseng, W.-C., Johnson Escauriza, A.J., Tsai-Morris, C.-H., Feldman, B., Dale, R.K., Wassif, C.A., Porter, F.D., 2021. The role of Niemann-Pick type C2 in zebrafish embryonic development. Development 148, dev194258. https://doi.org/10.1242/dev.194258

Udayar, V., Chen, Y., Sidransky, E., Jagasia, R., 2022. Lysosomal dysfunction in neurodegeneration: emerging concepts and methods. Trends Neurosci 45, 184–199. https://doi.org/10.1016/j.tins.2021.12.004

Varga, R.-E., Khundadze, M., Damme, M., Nietzsche, S., Hoffmann, B., Stauber, T., Koch, N., Hennings, J.C., Franzka, P., Huebner, A.K., Kessels, M.M., Biskup, C., Jentsch, T.J., Qualmann, B., Braulke, T., Kurth, I., Beetz, C., Hübner, C.A., 2015. In Vivo Evidence for Lysosome Depletion and Impaired Autophagic Clearance in Hereditary Spastic Paraplegia Type SPG11. PLoS Genet 11, e1005454. https://doi.org/10.1371/journal.pgen.1005454

Veeraval, L., O'Leary, C.J., Cooper, H.M., 2020. Adherens Junctions: Guardians of Cortical Development. Front Cell Dev Biol 8, 6. https://doi.org/10.3389/fcell.2020.00006

Wakabayashi, K., Gustafson, A.M., Sidransky, E., Goldin, E., 2011. Mucolipidosis type IV: an update. Mol Genet Metab 104, 206–213. https://doi.org/10.1016/j.ymgme.2011.06.006

Wong, C.-O., Li, R., Montell, C., Venkatachalam, K., 2012. Drosophila TRPML is required for TORC1 activation. Curr Biol 22, 1616–1621. https://doi.org/10.1016/j.cub.2012.06.055

Yang, S.-R., Kim, S.-J., Byun, K.-H., Hutchinson, B., Lee, B.-H., Michikawa, M., Lee, Y.-S., Kang, K.-S., 2006. NPC1 gene deficiency leads to lack of neural stem cell self-renewal and abnormal differentiation through activation of p38 mitogen-activated protein kinase signaling. Stem Cells 24, 292–298. https://doi.org/10.1634/stemcells.2005-0221

Yoon, S.-J., Elahi, L.S., Pașca, A.M., Marton, R.M., Gordon, A., Revah, O., Miura, Y., Walczak, E.M., Holdgate, G.M., Fan, H.C., Huguenard, J.R., Geschwind, D.H., Pașca, S.P., 2019. Reliability of human cortical organoid generation. Nat Methods 16, 75–78. https://doi.org/10.1038/s41592-018-0255-0

Yu, G., Wang, L.-G., Han, Y., He, Q.-Y., 2012. clusterProfiler: an R package for comparing biological themes among gene clusters. OMICS 16, 284–287. https://doi.org/10.1089/omi.2011.0118

Zhang, C., Liang, D., Ercan-Sencicek, A.G., Bulut, A.S., Cortes, J., Cheng, I.Q., Henegariu, O., Nishimura, S., Wang, X., Peksen, A.B., Takeo, Y., Caglar, C., Lam, T.T., Koroglu, M.N., Narayanan, A., Lopez-Giraldez, F., Miyagishima, D.F., Mishra-Gorur, K., Barak, T., Yasuno, K., Erson-Omay, E.Z., Yalcinkaya, C., Wang, G., Mane, S., Kaymakcalan, H., Guzel, A., Caglayan, A.O., Tuysuz, B., Sestan, N., Gunel, M., Louvi, A., Bilguvar, K., 2025. Dysregulation of mTOR signalling is a converging mechanism in lissencephaly. Nature 638, 172–181. https://doi.org/10.1038/s41586-024-08341-9

Zhong, X.Z., Sun, X., Cao, Q., Dong, G., Schiffmann, R., Dong, X.-P., 2016. BK channel agonist represents a potential therapeutic approach for lysosomal storage diseases. Sci Rep 6, 33684. https://doi.org/10.1038/srep33684

Zou, W., Lv, Y., Zhang, S., Li, L., Sun, L., Jiao, J., 2024. Lysosomal dynamics regulate mammalian cortical neurogenesis. Dev Cell 59, 64-78.e5. https://doi.org/10.1016/j.devcel.2023.11.021

Figure Legends

Figure 1. SPG11 neural progenitor cells (NPCs) feature altered lysosomal calcium.

A. Quantification of the DQ-BSA fluorescence intensity, indicative of lysosomal catalytic activity, in control and SPG11 NPCs. The graph shows the mean ± SEM. N>200 cells from 3 independent experiments. ns p>0.6. Unpaired T-test.
B. Control and SPG11 NPCs were immunostained with a LAMP1 antibody and with the GFP-D4 probe that labels cholesterol. Arrowheads point lysosomes. Scale bar: 10µm.
C. Quantification of the proportion of GFP-D4 staining colocalized with the marker LAMP1 in control and SPG11 NPCs, showing more cholesterol in lysosomes in SPG11 NPCs. The graph shows the mean ± SEM. N > 85 cells from three independent experiments. Unpaired t-test: *** p=0.0003.
D. Relative intensity of fluorescence detected by the calcium probe GCaMP3 addressed at the surface of lysosomes (GCaMP3-TRPML1) upon osmotic shock induced by 200 µM GPN in control and SPG11 NPCs. Osmotic shock induces the rupture of the lysosome membrane and the release of lysosomal calcium. The graph shows the mean ± SEM at each time point. N>35 cells from 3 independent experiments. Two-Way ANOVA. ** p=0.004.
E. Relative intensity of fluorescence detected by the calcium probe GCaMP3 addressed at the surface of lysosomes (GCaMP3-TRPML1) upon treatment with the TRPML1 agonist ML-SA1 (20 µM) in control and SPG11 NPCs. The graph shows the mean ± SEM at each time point. N>50 cells from 3 independent experiments. Two-Way ANOVA. ** p=0.01.
F. Quantification of the relative amount of lysosomal calcium monitored using the probe Oregon Green Bapta coupled to 10 kDa dextran in control and SPG11 NPCs, either untreated or treated for 24 hours with 20 µM ML-SA1. The graph shows the mean ± SEM. N=30 cells from 3 independent experiments. One-way ANOVA followed by Holm-Sidak's multiple comparisons test, *p=0.021, **p=0.004.

Figure 2. SPG11 neural progenitors in cortical organoids feature developmental impairments that are rescued by modulating lysosomal calcium channels.

A. Rosettes of control and SPG11 14-day old cortical organoids, either untreated or treated with ML-SA1. Samples were immunostained with antibodies against SOX2 for neural progenitors, ZO-1 for tight junctions, and LAMP1 as a marker for lysosomes. Scale bar: 50 µm.
B. Quantification of LAMP-1 fluorescence along a line scan perpendicular to the apical surface of rosettes in cortical organoids (white line on the inset image taken from panel A; ZO-1 in yellow,

LAMP1 in magenta), indicating lysosome localization in neural progenitors. The graph shows the mean ± SEM. N=30 rosettes from 3 independent experiments.

C. Rosettes of control and SPG11 14-day-old cortical organoids, either untreated or treated with ML-SA1, were immunostained with antibodies against SOX2 for neural progenitors as well as LAMP1 for lysosomes and were stained with the GFP-D4 probe to detect cholesterol. Note that cholesterol accumulates mainly in lysosomes in untreated SPG11 cortical organoids (arrowheads) Scale bar: 20 µm.

D. Quantification of the proportion of GFP-D4 staining that is colocalized with lysosomes (LAMP1 immunostaining). The graph shows the mean ± SEM. N>40 rosettes from 3 independent experiments. One-way ANOVA followed by Holm-Sidak's multiple comparisons test. ****p<0.0001.

E. Immunostaining of rosettes in control and SPG11 14-day-old cortical organoids, either untreated or treated with ML-SA1, with antibodies against SOX2 for neural progenitors and Ki67 for dividing cells. Scale bar: 50 µm

F. Quantification of the number of SOX2 positive progenitor cells per rosette in control and SPG11 organoids that were untreated or treated with ML-SA1. The graph shows the mean ± SEM. N>35 rosettes from 3 independent experiments. One-way ANOVA followed by Holm-Sidak's multiple comparisons test. ****p<0.0001.

G. Quantification of the proportion of SOX2 positive cells that were also positive for the Ki67 marker in control and SPG11 organoids that were untreated or treated with ML-SA1. The graph shows the mean ± SEM. N=30 rosettes from 3 independent experiments. One-way ANOVA followed by Holm-Sidak's multiple comparisons test. ****p<0.0001.

Figure 3. Later stage SPG11 cortical organoids show normal proliferation and tight junctions but feature reduced cortical lamination that can be improved with ML-SA1 treatment.

A. Rosettes of control and SPG11 42-day-old cortical organoids were immunostained with antibodies against SOX2 for neural progenitors, ZO-1 for tight junctions, and Ki-67 as a marker for proliferation. Scale bar: 50 µm.

B. Quantification of the proportion of SOX2 positive cells that were also positive for the Ki67 marker in 42-day-old control and SPG11 cortical organoids. The graph shows the mean ± SEM. N=30 rosettes from 3 independent experiments. Unpaired T-test, ns: p=0.69

C. Quantification of ZO-1 fluorescence along a line scan perpendicular to the apical surface of randomly selected rosettes in 42-day-old control and SPG11 cortical organoids, indicating tight

junction enrichment in neural progenitors. The graph shows the mean ± SEM. N=30 rosettes from 3 independent experiments.

D. Rosettes in 42-day-old control and SPG11 cortical organoids, either untreated or treated with ML-SA1, were immunostained with antibodies against SOX2 for neural progenitors, TBR2 for intermediate progenitors, and NeuN for neurons. Arrowhead point intermediate progenitors and stars point neurons. Scale bar: 100 µm.

E. - G Quantification of the number of SOX2- (E), TBR1- (F) or NeuN-positive (G) cells in rosettes of 42-day-old control and SPG11 cortical organoids, either untreated or treated with ML-SA1. The graphs show the mean ± SEM. N>30 rosettes from 3 independent experiments. One-way ANOVA followed by Holm-Sidak's multiple comparisons test, **p<0.01; ***p<0.001; ****p<0.0001.

Figure 4. Inhibition of the mTOR pathway contributes to impaired proliferation of neural progenitors in SPG11 cortical organoids.

A. Rosettes in control and SPG11 14-day-old cortical organoids, either untreated or treated with ML-SA1, were immunostained with antibodies against SOX2 for neural progenitors, and phosphorylated S6. Scale bar: 50 µm.

B. Quantification of the relative levels of intensity of phosphorylated S6 in rosettes of control and SPG11 cortical organoids, either untreated or treated with ML-SA1. Values were normalized to the average fluorescence of phosphorylated S6 staining of controls in each experiment. The graph shows the mean ± SEM. N=30 rosettes from 3 independent experiments. One-way ANOVA followed by Holm-Sidak's multiple comparisons test, ***p<0.001; ****p<0.0001.

C. Quantification of the relative levels of intensity of fluorescence of phosphorylated S6 in rosettes of control and SPG11 14-day-old cortical organoids, either untreated or treated with the mTOR agonist NV5138 (100µM). Values were normalized to the average phosphorylated S6 fluorescence of controls in each experiment. The graph shows the mean ± SEM. N>25 rosettes from 3 independent experiments. One-way ANOVA followed by Holm-Sidak's multiple comparisons test, *p=0.016;****p<0.0001.

D. Immunostaining of rosettes in 14-day-old control and SPG11 organoids, either untreated or treated with NV5138, with antibodies against SOX2 for neural progenitors, KiI67 for dividing cells, and ZO-1 to label tight junctions. Scale bar: 20 µm

E. Quantification of the proportion of SOX2 positive cells that were also positive for the Ki67 marker in control and SPG11 organoids that were untreated or treated with NV5138. The graph shows the mean ± SEM. N>25 rosettes from 3 independent experiments. One-way ANOVA followed by Holm-Sidak's multiple comparisons test. **p=0.008; ****p<0.0001.

F. Quantification of ZO-1 fluorescence along a line scan perpendicular to the apical surface of randomly selected rosettes in 14-day-old control and SPG11 cortical organoids, either untreated or treated with NV5138. The graph shows the mean ± SEM. N>35 rosettes from 3 independent experiments. Note the decrease in the intensity of ZO-1 immunostaining at the apical surface of SPG11 rosettes, which is compensated in the presence of NV5138 treatment.

Figure 5. ML-SA1 restores mTOR signaling in SPG11 cells by modulating lysosomal levels of phosphatidylinositol-4-phosphate (PI(4)P).

A. Western blots showing levels of phosphorylated S6 (PS6), total S6 protein, as well as GAPDH in control and SPG11 NPCs, either untreated or treated with 20 µM ML-SA1 for 24 hours.
B. Quantification of the ratio of phosphorylated to total levels of S6 (PS6/S6 ratio) in control and SPG11 NPCs, either untreated or treated with ML-SA1. The graph shows the mean ± SEM. N=8 cell sample preparations from 5 independent experiments. One-way ANOVA followed by Holm-Sidak's multiple comparisons test, **p<0.01.
C. Immunostaining of control and SPG11 NPCs, either untreated or treated with ML-SA1 for 24 hours, with antibodies against LAMP1 labelling lysosomes and mTOR. Scale bar: 10 µm.
D. Quantification of the proportion of mTOR immunostaining that is colocalized with lysosomes (LAMP1 immunostaining). The graph shows the mean ± SEM. N> 44 transfected cells from 3 independent experiments. One-way ANOVA followed by Holm-Sidak's multiple comparisons test, ** p<0.01; ****p<0.0001.
E. Live spinning disk confocal images of control and SPG11 NPCs, either untreated or treated with ML-SA1 for 24 hours, and transfected with vectors allowing expression of the lysosomal marker Lamp1-mCherry and the reporter of PI(4)P GFP-P4MsidMx2. Scale bar: 10 µm.
F. Quantification of the GFP-P4MsidMx2 fluorescence intensity in Lamp1-mCherry mask normalized by the cytosolic levels in control and SPG11 NPCs, either untreated or treated with ML-SA1. The graph shows the mean ± SEM. N>40 transfected cells from 3 independent experiments. One-way ANOVA followed by Holm-Sidak's multiple comparisons test, ****p<0.0001.
G. Rosettes in 14-day-old control and SPG11 cortical organoids, either untreated or treated with ML-SA1, were immunostained with antibodies against LAMP1 and PI4K2A, as well as stained with DAPI. Scale bar: 20 µm.
H. Quantification of the proportion of PI4K2A colocalized with lysosomes in rosettes of control or SPG11 organoids, either untreated or treated with ML-SA1. The graph shows the mean ± SEM.

N>30 rosettes from 3 independent experiments. One-way ANOVA followed by Holm-Sidak's multiple comparisons test, ****p<0.0001.

I. Quantification of the proportion of PI4K2A colocalized with lysosomes in rosettes of control organoids, either untreated or treated with ML-SI1. The graph shows the mean ± SEM. N>30 rosettes from 3 independent experiments. Unpaired T-test, ***p=0.0009.

Supplementary Figure 1. Lysosome catabolic activity is preserved in SPG11 NPCs

A. Quantification of Magic Red Fluorescent Cathepsin B assay performed on control and SPG11 NPCs. The graph shows the mean ± SEM. N=7 wells (with >200 cells analyzed per well) of a 24-well plate from 3 independent experiments. ns p=0.19. Unpaired t-test.
B. Western blots showing expression levels of the lysosomal proteins LAMP1 and Cathepsin D. For the latter, note the presence of full length, unprocessed Cathepsin D (Cath D), and the cleaved mature Cathepsin D (Mat. Cath D).
C. D. Quantification of the relative levels of the mature form of Cathepsin D and LAMP1, normalized to levels of β-tubulin. The graphs show the mean ± SEM. N=7 independent experiments. ns p>0.24 Unpaired t-test.
E. Live confocal image of NPCs loaded for 16 hours with 10 kDa dextran Texas Red and 10 kDa dextran coupled to the calcium probe Oregon Green 488 Bapta and stained with Lysotracker blue. Dashed line indicates the cell periphery. Note the colocalization of 10 kDa dextran probes with Lysotracker. Scale bar: 5 µm.

Supplementary Figure 2. Altering lysosomal calcium in cortical organoids impairs neural progenitor proliferation

A. Quantification of the mean intensity of GFP-D4 fluorescence per rosette in control and SPG11 cortical organoids, either untreated or treated with ML-SA1. The graph shows the mean ± SEM. N>40 rosettes from 3 independent experiments. One-way ANOVA followed by Holm-Sidak's multiple comparisons test. **p<0.01
B. Quantification of ZO-1 fluorescence along a line scan perpendicular to the apical surface of randomly selected rosettes in control and SPG11 14-day-old cortical organoids, either untreated or treated with ML-SA1, indicating tight junction enrichment in neural progenitors. The graph shows the mean ± SEM. N=30 rosettes from 3 independent experiments. Note the decrease in the intensity of ZO-1 immunostaining at the apical surface of SPG11 rosettes, which is compensated in the presence of ML-SA1 treatment.
C. Rosettes of control 14-day-old cortical organoids, either untreated or treated with the TRPML1 antagonist ML-SI1 were immunostained with antibodies against SOX2 for neural progenitors, Ki67 for proliferating cells and ZO-1 for tight junctions. Scale bar: 50 µm.
D. Quantification of the proportion of SOX2-positive cells that were also positive for the Ki67 marker in control organoids that were untreated or treated with ML-SI1. The graph shows the mean ± SEM. N=30 rosettes from 3 independent experiments. Unpaired t-test, ****p<0.0001.

E. Quantification of ZO-1 fluorescence along a line scan perpendicular to the apical surface of randomly selected rosettes in control 14-day-old cortical organoids, either untreated or treated with ML-SI1. The graph shows the mean ± SEM. N=30 rosettes from 3 independent experiments.

Supplementary Figure 3. ML-SA1 treatment modulates transcription in SPG11 cortical organoids

A. Volcano plot depicting differential gene expression of transcriptomes between SPG11 and control 14-day-old cortical organoids (N=4). Genes significantly upregulated in SPG11 organoids are orange, while significantly downregulated genes are blue. EdgeR analysis using log2FC > 1, FDR < 0.05. Covariate corrections performed to account for experiments launched separately.
B. Volcano plots depicting differential gene expression of transcriptomes between untreated and ML-SA1 treated SPG11 14-day-old cortical organoids (N=4). Genes significantly upregulated by ML-SA1-treated organoids are orange, while significantly downregulated genes are blue. EdgeR analysis using log2FC > 1, FDR < 0.05. Covariate corrections performed to account for experiments launched separately.
C. Summary of geneset enrichment analysis (GSEA) results using the MsigDB Hallmark database showing pathways with an adjusted p-value <0.05.
D. Rosettes in control and SPG11 14-day-old cortical organoids, either untreated or treated with NV5138, were stained with DAPI and immunostained with antibodies against phosphorylated S6. Scale bar: 20 µm.

Supplementary Figure 4. ML-SA1 treatment modulates PI4K2A lysosomal localization in SPG11 NPCs

A. Immunostaining of control or SPG11 NPCs, either untreated or treated with ML-SA1, with antibodies raised against PI4K2A and LAMP1 to stain lysosomes. Scale bar: 10 µm.
B. Quantification of the proportion of PI4K2A signal colocalized with lysosomes labelled by LAMP1 immunostaining in control or SPG11 NPCs, either untreated or treated with ML-SA1 for 24 hours. The graph shows the mean ± SEM. N>50 NPCs analyzed from 3 independent experiments. Ordinary one-way ANOVA followed by Holm-Sidak's multiple comparisons test. ****p<0.0001.

Figure 1

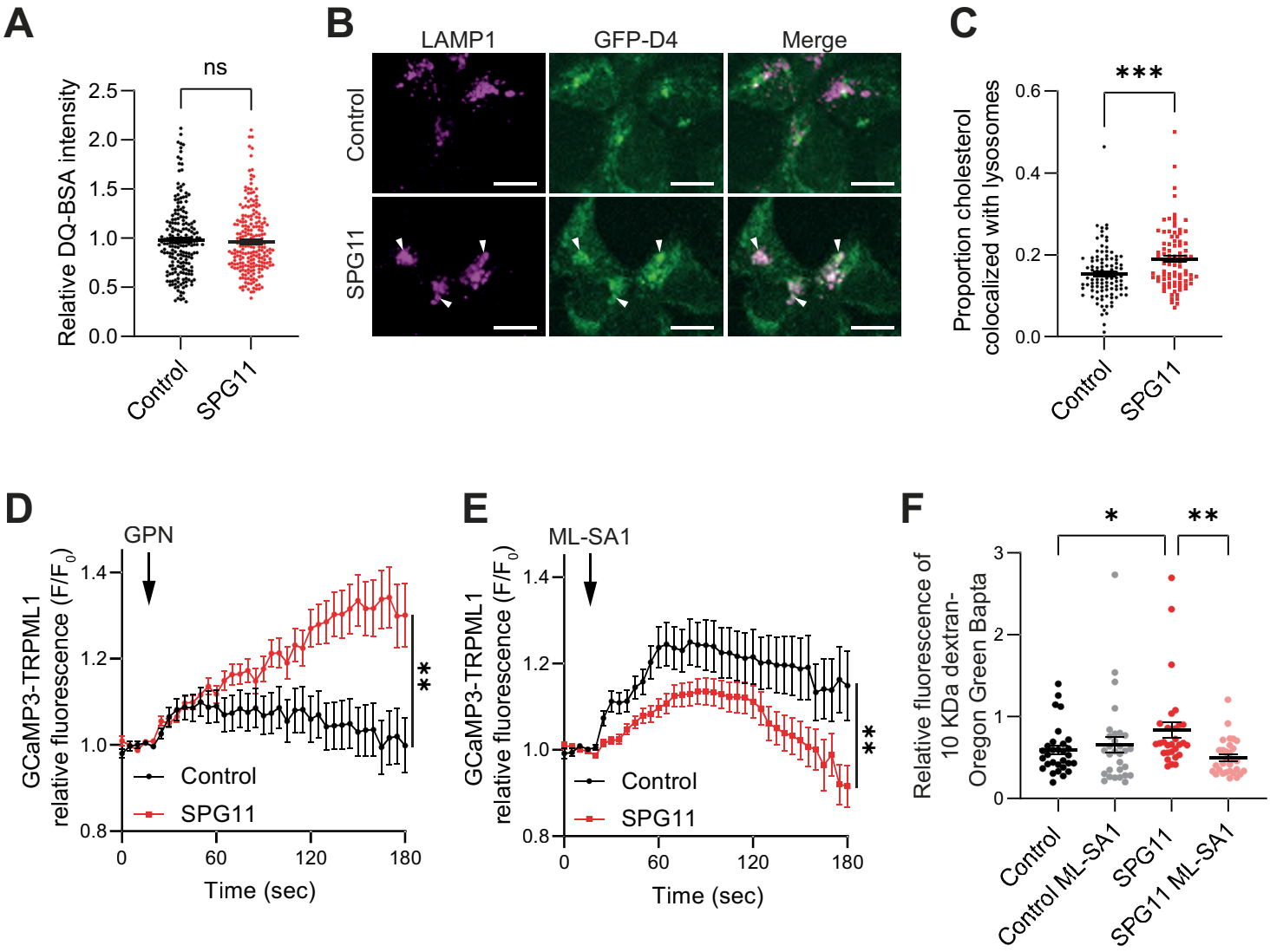
A
ns
Relative DQ-BSA intensity
2.5
2.0
1.5
1.0
0.5
0.0
Control
SPG11
B
LAMP1
GFP-D4
Merge
Control
SPG11
C
***
Proportion cholesterol colocalized with lysosomes
0.6
0.4
0.2
0.0
Control
SPG11
D
GPN
GCaMP3-TRPML1 relative fluorescence (F/F0)
1.4
1.2
1.0
0.8
**
Control
SPG11
0
60
120
180
Time (sec)
E
ML-SA1
GCaMP3-TRPML1 relative fluorescence (F/F0)
1.4
1.2
1.0
0.8
**
Control
SPG11
0
60
120
180
Time (sec)
F
*
**
Relative fluorescence of 10 KDa dextran-Oregon Green Bapta
3
2
1
0
Control
Control ML-SA1
SPG11
SPG11 ML-SA1

Figure 2

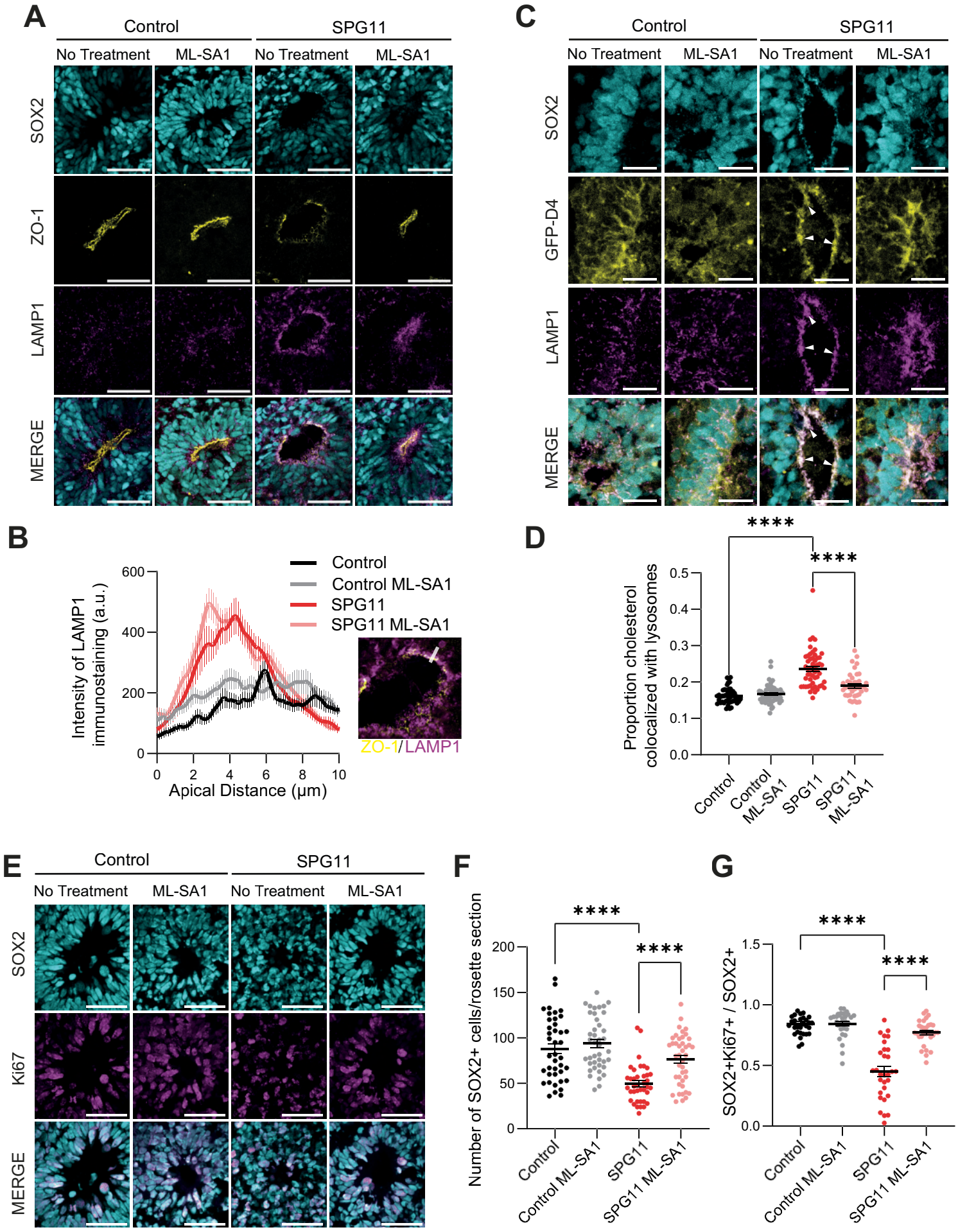
A
Control
SPG11
No Treatment
ML-SA1
No Treatment
ML-SA1
SOX2
ZO-1
LAMP1
MERGE
C
Control
SPG11
No Treatment
ML-SA1
No Treatment
ML-SA1
SOX2
GFP-D4
LAMP1
MERGE
B
Control
Control ML-SA1
SPG11
SPG11 ML-SA1
Intensity of LAMP1 immunostaining (a.u.)
600
400
200
0
0
2
4
6
8
10
Apical Distance (µm)
ZO-1/LAMP1
D
****
****
Proportion cholesterol colocalized with lysosomes
0.5
0.4
0.3
0.2
0.1
0.0
Control
Control ML-SA1
SPG11
SPG11 ML-SA1
E
Control
SPG11
No Treatment
ML-SA1
No Treatment
ML-SA1
SOX2
Ki67
MERGE
F
****
****
Number of SOX2+ cells/rosette section
200
150
100
50
0
Control
Control ML-SA1
SPG11
SPG11 ML-SA1
G
****
****
SOX2+Ki67+ / SOX2+
1.5
1.0
0.5
0.0
Control
Control ML-SA1
SPG11
SPG11 ML-SA1

Figure 3

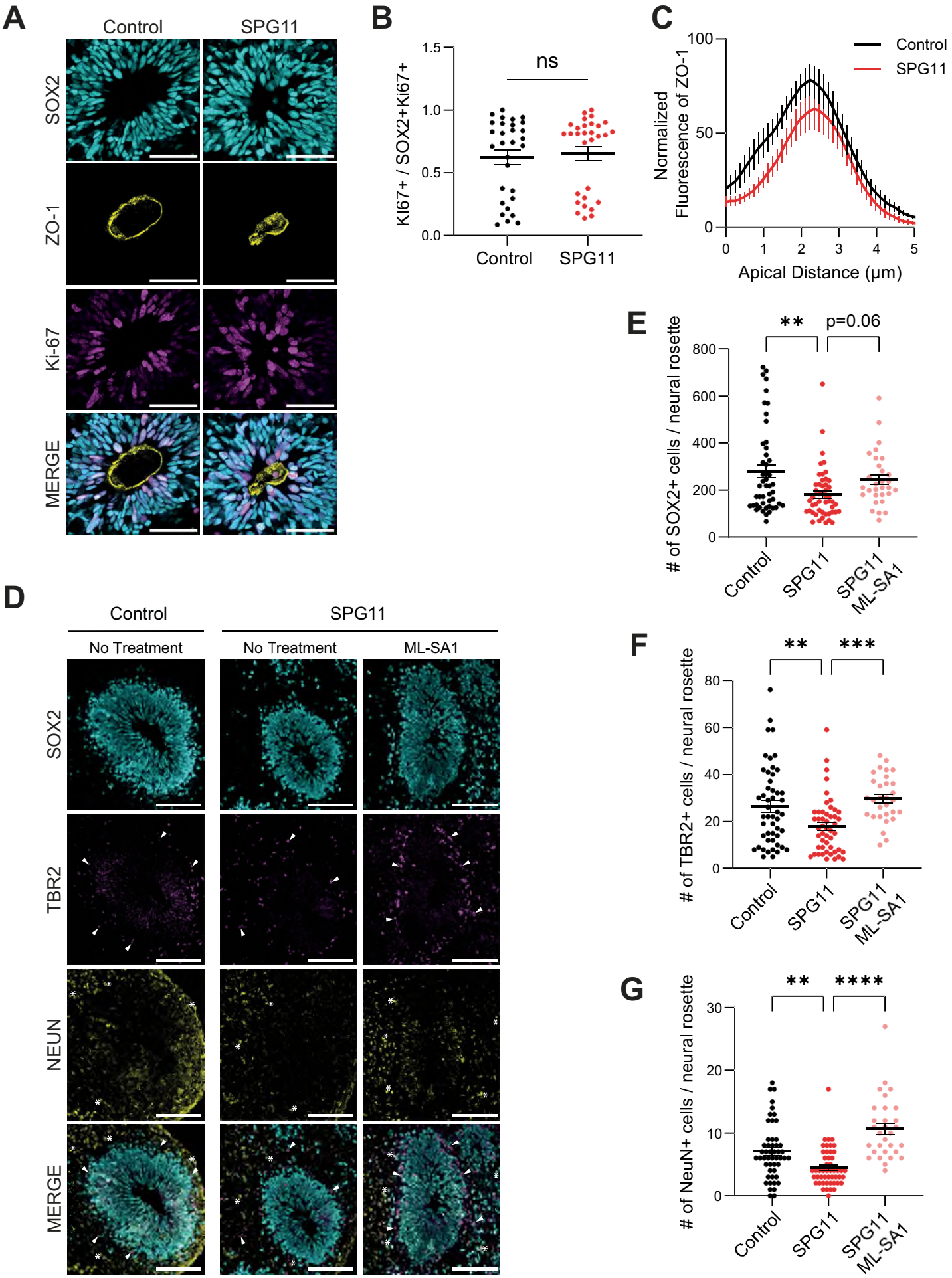
A
Control
SPG11
SOX2
ZO-1
Ki-67
MERGE
B
ns
Ki67+ / SOX2+Ki67+
1.5
1.0
0.5
0.0
Control
SPG11
C
Control
SPG11
Normalized Fluorescence of ZO-1
100
50
0
0
1
2
3
4
5
Apical Distance (µm)
E
**
p=0.06
# of SOX2+ cells / neural rosette
800
600
400
200
0
Control
SPG11
SPG11 ML-SA1
D
Control
SPG11
No Treatment
No Treatment
ML-SA1
SOX2
TBR2
NEUN
MERGE
F
**
***
# of TBR2+ cells / neural rosette
80
60
40
20
0
Control
SPG11
SPG11 ML-SA1
G
**
****
# of NeuN+ cells / neural rosette
30
20
10
0
Control
SPG11
SPG11 ML-SA1

Figure 4

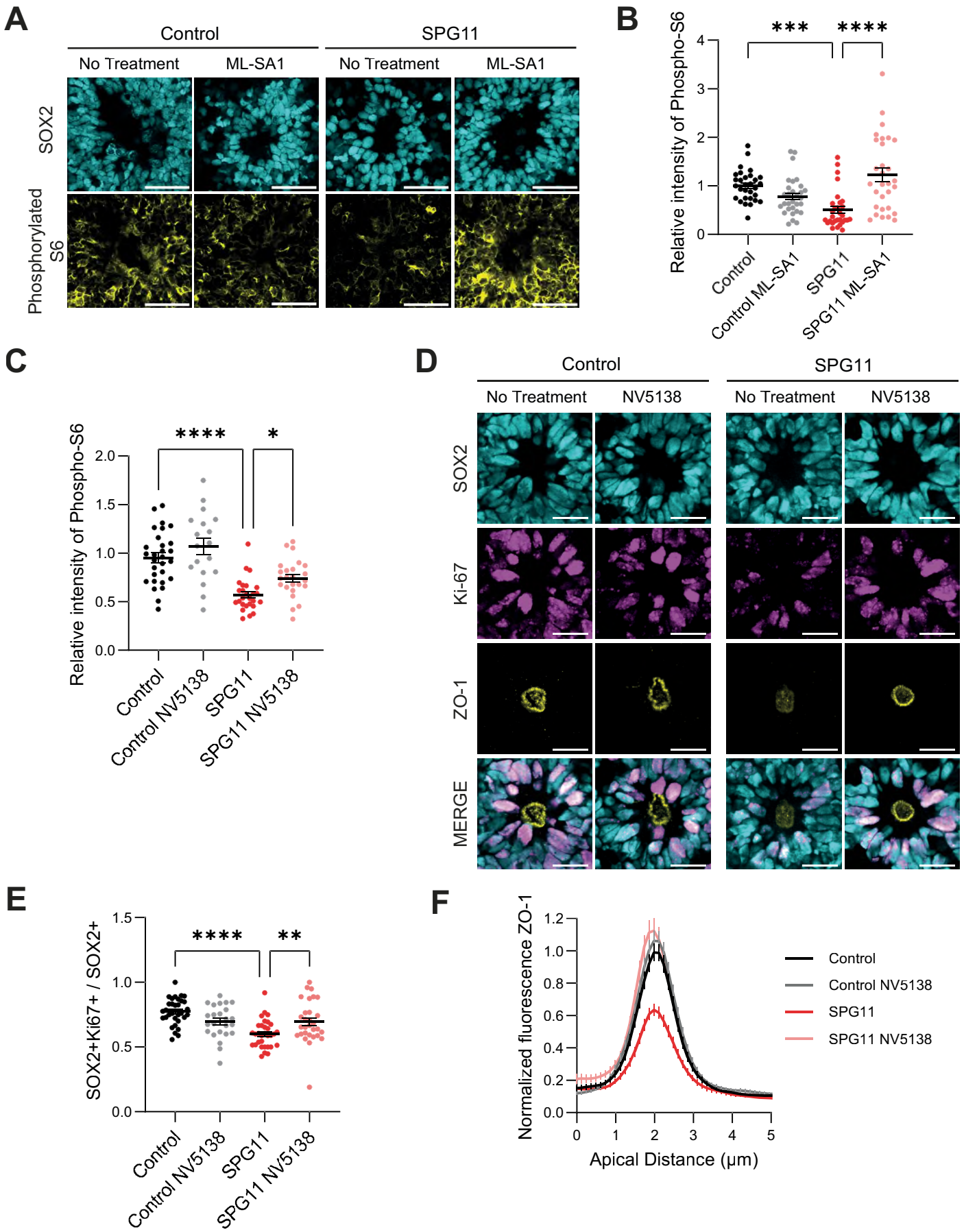
A
Control
SPG11
No Treatment
ML-SA1
No Treatment
ML-SA1
SOX2
Phosphorylated S6
B
Relative intensity of Phospho-S6
***
****
Control
Control ML-SA1
SPG11
SPG11 ML-SA1
C
Relative intensity of Phospho-S6
****
*
Control
Control NV5138
SPG11
SPG11 NV5138
D
Control
SPG11
No Treatment
NV5138
No Treatment
NV5138
SOX2
Ki-67
ZO-1
MERGE
E
SOX2+Ki67+ / SOX2+
****
**
Control
Control NV5138
SPG11
SPG11 NV5138
F
Normalized fluorescence ZO-1
Apical Distance (µm)
Control
Control NV5138
SPG11
SPG11 NV5138

Figure 5

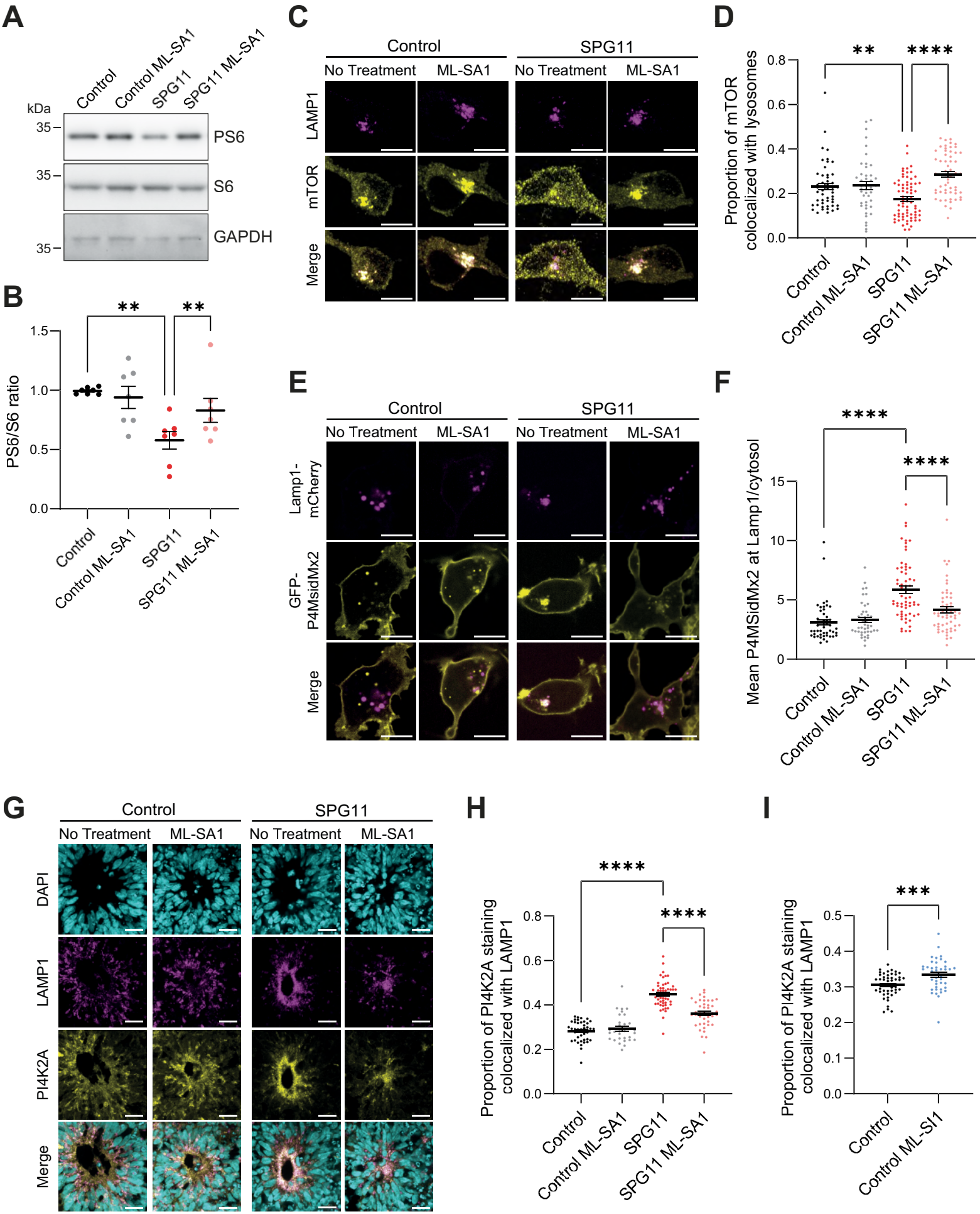
A
Control
Control ML-SA1
SPG11
SPG11 ML-SA1
kDa
35
PS6
S6
GAPDH
B
PS6/S6 ratio
1.5
1.0
0.5
0.0
**
**
Control
Control ML-SA1
SPG11
SPG11 ML-SA1
C
Control
SPG11
No Treatment
ML-SA1
LAMP1
mTOR
Merge
D
Proportion of mTOR colocalized with lysosomes
0.8
0.6
0.4
0.2
0.0
**
****
E
Lamp1-mCherry
GFP-P4MsidMx2
F
Mean P4MSidMx2 at Lamp1/cytosol
15
10
5
0
****
G
DAPI
PI4K2A
H
Proportion of PI4K2A staining colocalized with LAMP1
I
***
Control ML-SI1

Supplementary Figure 1

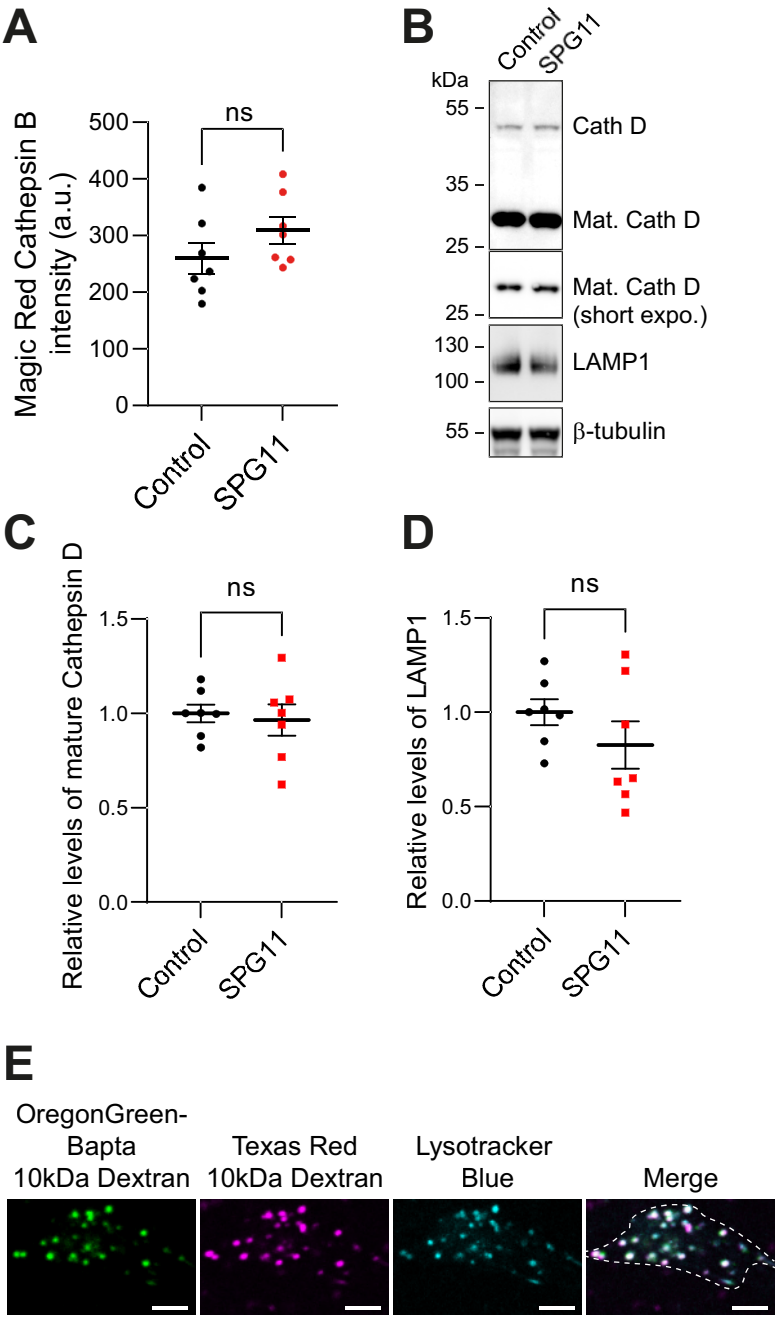

Supplementary Figure 2

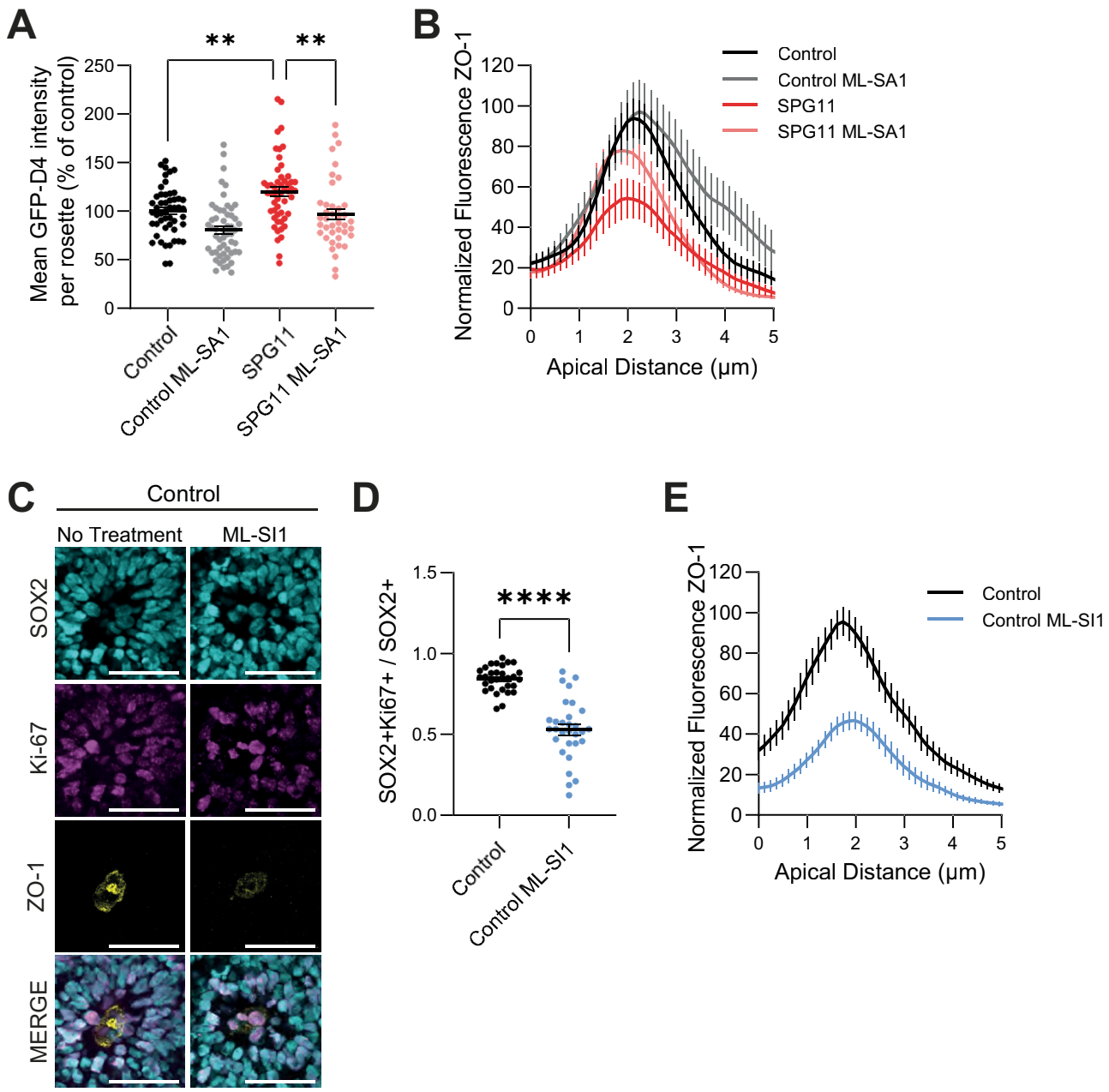

Supplementary Figure 3

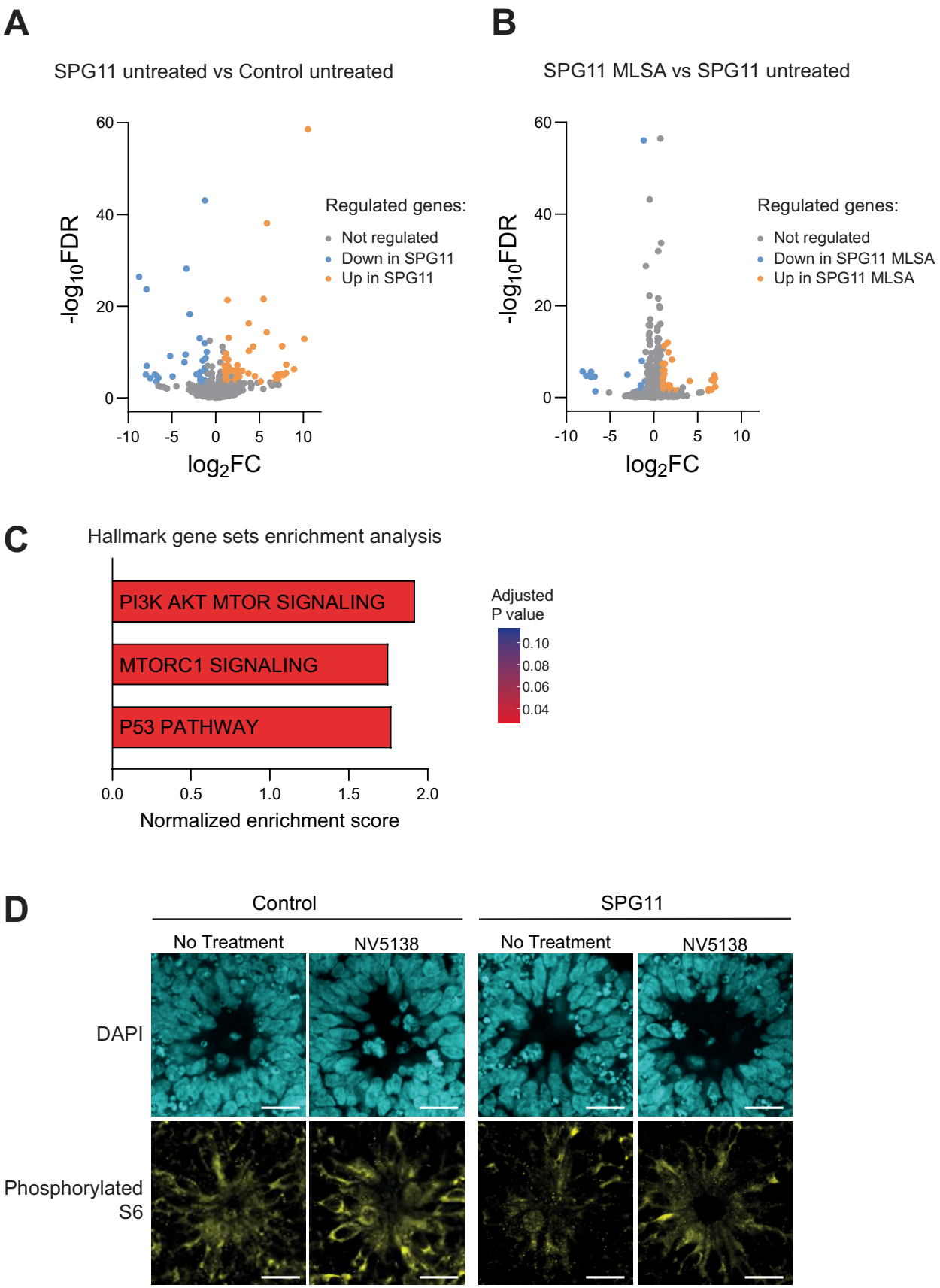
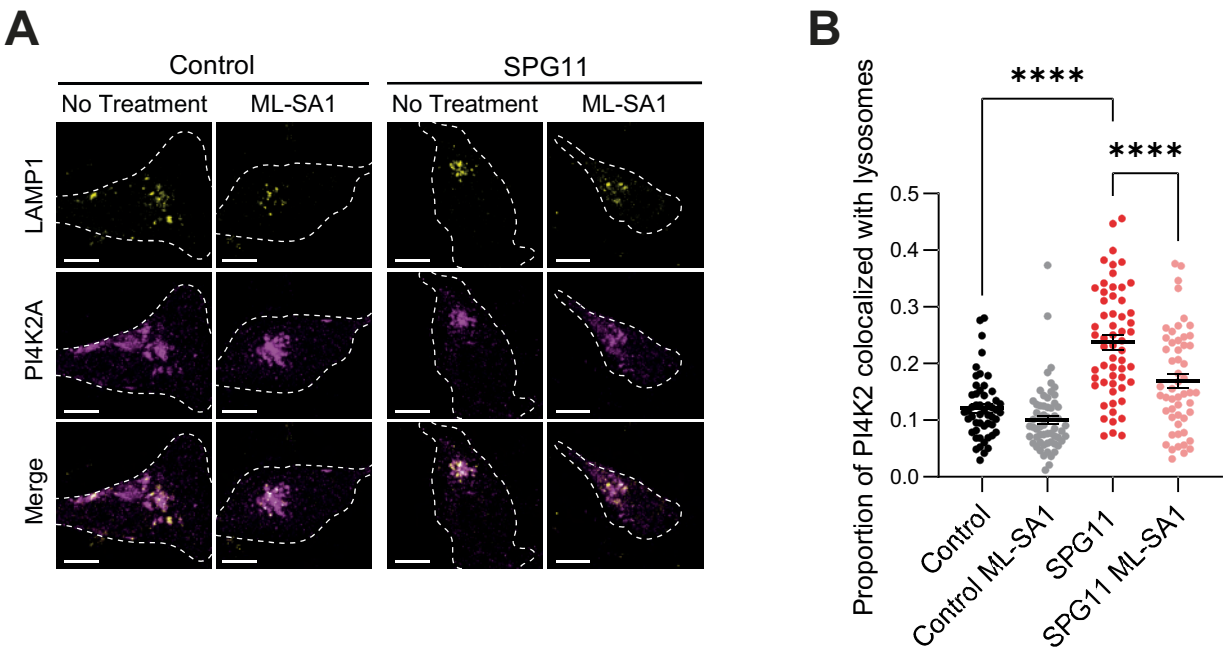
Supplementary Figure 4